TCAB1 prevents nucleolar accumulation of the telomerase RNA to promote telomerase assembly

Basma S. Al-Masraf [1,2,3], Gloria I. Perez [1], Kate Adams-Boone [1], Scott B. Cohen [4], Li Han [5], Kefei Yu [5], Jens C. Schmidt [1,6,*]

[1] Institute for Quantitative Health Sciences and Engineering, Michigan State University, East Lansing, MI, U.S.A.

[2] College of Osteopathic Medicine, Michigan State University, East Lansing, MI, U.S.A.

[3] Cellular and Molecular Biology Graduate Program, College of Natural Sciences, Michigan State University, East Lansing, MI, U.S.A.

[4] Children's Medical Research Institute and University of Sydney, Westmead, NSW 2145, Australia.

[5] Department of Microbiology and Molecular Genetics, Michigan State University, East Lansing, MI, U.S.A.

[6] Department of Obstetrics, Gynecology, and Reproductive Biology, Michigan State University, East Lansing, MI, U.S.A.

[*] Correspondence: schmi706@msu.edu

Abstract

Localization of a wide variety of RNAs to non-membrane bound cellular compartments such as nucleoli, Cajal bodies, and stress-granules is critical for their function and stability. The molecular mechanisms that underly the recruitment and exclusion of specific RNAs from these phase-separated organelles is poorly understood. Telomerase is a ribonucleoprotein (RNP), that is composed of the reverse transcriptase protein TERT, the telomerase RNA (TR), and several auxiliary proteins that associate with TR, including TCAB1. Here we show that, that in the absence of TCAB1, TR is sequestered in the nucleolus, while TERT localizes to the nucleoplasm and is excluded from the nucleolus, which prevents telomerase assembly. Thus, nuclear compartmentalization by the non-membrane bound nucleolus counteracts telomerase assembly and TCAB1 is required to exclude the telomerase RNA from the nucleolus. Our work provides general insight into the mechanism and functional consequences of RNA recruitment to organelles formed by phase-separation and proposes a new model explaining the critical role of TCAB1 in telomerase function.

Introduction

Human cells contain a number of non-membrane bound organelles that carry out critical cellular functions. For instance, nucleoli and Cajal bodies are phase-separated nuclear organelles that play important roles in the biogenesis and maturation of many cellular RNAs (Hyman et al., 2014; Mitrea and Kriwacki, 2016). Nucleoli and Cajal bodies contain a wide range of small nucleolar and small Cajal body-specific RNAs (snoRNAs and scaRNAs, respectively). A subset of these snoRNAs and scaRNAs are bound by the H/ACA complex, which contains NOP10, NHP2, GAR1, and the pseudouridylase dyskerin, which modifies ribosomal and spliceosomal RNA precursors and other RNAs (Angrisani et al., 2014). A key difference between snoRNAs and scaRNAs is the presence of the Cajal-body box (CAB-box) motif in scaRNAs that directly associates with the telomerase Cajal body protein 1 (TCAB1, also known as WRAP53) (Jády et al., 2004; Schmidt and Cech, 2015; Venteicher et al., 2009). TCAB1 is required for the recruitment of scaRNAs to Cajal bodies and in its the absence scaRNAs localize to the nucleolus (Tycowski et al., 2009). Therefore, TCAB1 controls which phase-separated nuclear organelle scaRNAs associate with. Importantly, the molecular mechanism by which TCAB1 drives exclusion of scaRNAs from the nucleolus and facilitates their recruitment to Cajal bodies is unknown. In addition, it is unclear whether miss-localization of scaRNAs to the nucleolus has functional consequences.

The telomerase RNA (TR) is a scaRNA and like other scaRNAs its association with nucleoli and Cajal bodies is controlled by TCAB1 (Schmidt and Cech, 2015). Telomere maintenance by telomerase is essential for continuous proliferation of stem cell

populations in the human body and most cancers require telomerase activity for their survival (Stewart and Weinberg, 2006). To compensate for the incomplete replication of chromosome ends, telomerase appends TTAGGG repeats to the telomeric single-stranded overhang (Schmidt and Cech, 2015). Telomerase-mediated telomere maintenance requires three critical steps: Telomerase assembly, telomerase recruitment to telomeres, and telomeric repeat synthesis (Schmidt and Cech, 2015). Mutations in several genes have been identified that cause deficiencies in one of these critical steps and lead to a variety of diseases known as telomere syndromes, characterized by premature depletion of stem cell populations (Armanios and Blackburn, 2012). In addition, telomerase is inappropriately activated in >85% of cancers (Stewart and Weinberg, 2006). While telomerase recruitment to telomeres (Nandakumar and Cech, 2013) and telomerase catalysis (Wu et al., 2017) have been studied extensively, much less is known about telomerase assembly. Importantly, telomerase assembly could be targeted to reduce telomerase activity in cancer cells, or to increase telomerase function in patients affected by genetically defined telomerase deficiency syndromes (Nagpal et al., 2020; Shukla et al., 2020).

Telomerase is a complex ribonucleoprotein (RNP). The core components of telomerase are the telomerase reverse transcriptase (TERT) protein, TR, the H/ACA complex, and TCAB1 (Schmidt and Cech, 2015). The primary function of the H/ACA complex is to stabilize TR, by directly binding to its 3'-end, preventing the exonucleolytic degradation of TR (Stuart et al., 2015; Tummala et al., 2015). The 3'-end formation of TR is tightly regulated by the competing activities of the poly-(A) polymerase PAPD5 and the nuclease

PARN (Shukla et al., 2016; Tseng et al., 2015). Loss of TCAB1 function leads to telomere attrition in a variety of cell lines (Chen et al., 2018; Venteicher et al., 2009; Vogan et al., 2016; Zhong et al., 2011). In addition, multiple mutations in TCAB1 have been identified that cause misfolding of TCAB1 and lead to dyskeratosis congenita, a telomere syndrome (Freund et al., 2014; Zhong et al., 2011). While these observations highlight that TCAB1 is necessary for telomere maintenance, the underlying molecular mechanism is unclear. Initially, it was proposed that TCAB1 is required for telomerase recruitment to telomeres (Stern et al., 2012; Venteicher et al., 2009). A more recent study suggested that TCAB1 is required for the correct folding of TR, and that its absence causes a reduction in telomerase activity (Chen et al., 2018). Importantly, all previous studies have come to the conclusion that TCAB1 is not required for telomerase assembly.

Here we analyze telomerase assembly in intact cells and by purification of the telomerase RNP and demonstrate that, contrary to previous findings, TCAB1 promotes telomerase assembly *in vivo.* Using a combination of genetic perturbations, biochemical analysis of telomerase function, cell biological approaches, and single-molecule live cell imaging, we show that in the absence of TCAB1, TR is sequestered in the nucleolus while TERT is excluded from the nucleolus. The spatial separation of TERT and TR that we observe in our experiments is inconsistent with proper telomerase assembly. Furthermore, we show that the limited amount of telomerase that can assemble in the absence of TCAB1 is fully active and can localize to telomeres, suggesting that TCAB1 is not necessary for the enzymatic function of telomerase or its recruitment to telomeres. We conclude that the sequestration of TR in the nucleolus, when TCAB1 is absent, prevents its association with

TERT, and that this lack of telomerase assembly is the molecular mechanism underlying the critical role of TCAB1 in telomere maintenance. Our results also demonstrate that the nucleolar phase separation constitutes a barrier for telomerase assembly and suggest that incompletely assembled RNPs are tightly associated with the nucleolus and do not readily enter the nucleoplasm.

Results

Loss of TCAB1 leads to nucleolar accumulation of TR

To confirm that TR is sequestered in the nucleolus in the absence of TCAB1, we knocked out TCAB1 in HeLa cells and HeLa cells expressing 3xFLAG-HaloTag-TERT (Halo-TERT) using Cas9 with two guide RNAs to delete exons 2 and 3 from the TCAB1 gene, which removes the coding sequence for residues 144-214 of TCAB1 and results in a frame shift (Figure 1 – figure supplement 1). TCAB1 knock-out was validated by Southern blot, PCR, Western blot, and immunofluorescence imaging (IF, Fig. 1A-C, Figure 1 – figure supplement 1). To assure that no truncated form of TCAB1 was expressed in TCAB1 knock-out cells, we assessed TCAB1 expression using two antibodies, targeting the N-terminus and C-terminus of TACB1, respectively (Figure 1 – figure supplement 1). TCAB1 knock-out cells continuously grew at approximately 60% of the rate of their parental cell lines (Figure 1 – figure supplement 1). Telomeres in cells lacking TCAB1 were stable at a shorter length than their parental control, as previously described (Vogan et al., 2016). Fluorescence *in situ* hybridization (FISH) demonstrated that TR accumulates in the nucleolus in cells that lack TCAB1, as indicated by co-localization of TR and nucleolar dyskerin signals. Importantly, expression of GFP-TCAB1 in TCAB1 knock-out cells rescued TR localization to Cajal bodies (Figure 1 – figure supplement 1), confirming that the miss-localization of TR to nucleoli is caused by absence of TCAB1. These observations demonstrate that TCAB1 is required to prevent TR accumulation in the nucleolus.

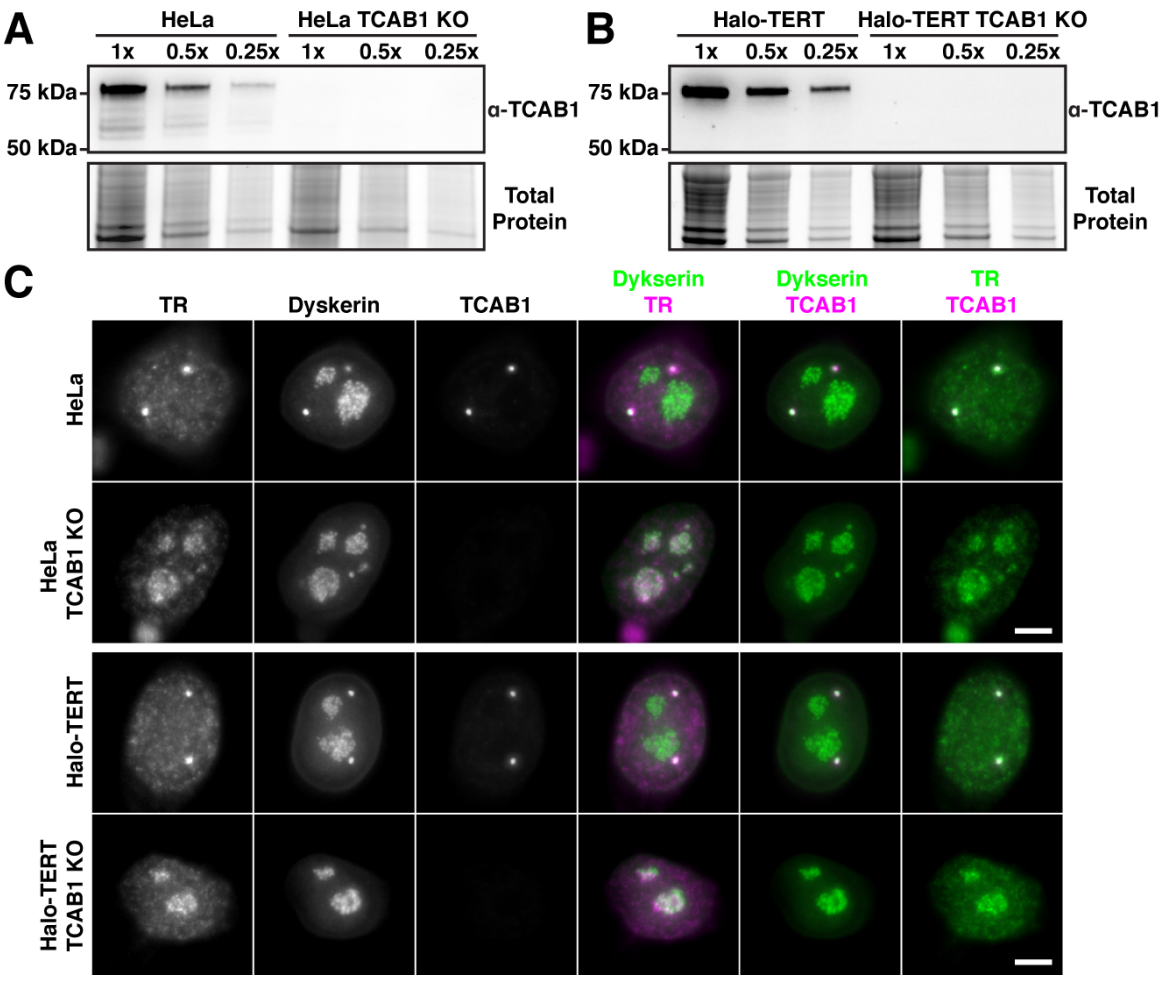

Figure 1. TR is localized to nucleoli in TCAB1 knock-out cells. (A-B) Western blot demonstrating the absence of TCAB1 protein in TCAB1 knock-out cell lines generated from **(A)** HeLa and **(B)** Halo-TERT parental cell lines (probed with Proteintech TCAB1 antibody). **(C)** Immuno-fluorescence with anti-dyskerin and anti-TCAB1 antibodies coupled to fluorescence in-situ hybridization with probes against TR, demonstrating the absence of TCAB1 and TR localization to nucleoli in TCAB1 knock-out cells (scale bar = 5 μm).

TERT is excluded from nucleoli

Our previous observations demonstrated that TERT does not enter nucleoli in human cancer cells (Schmidt et al., 2016). To confirm these results, we performed single-molecule imaging of 3xFLAG-HaloTag-TERT in living HeLa cells. Consistent with our previous results, 3xFLAG-HaloTag-TERT was not observed entering or overlapping with

nucleoli, which are discernible as circular shapes in the nucleus under transmitted light

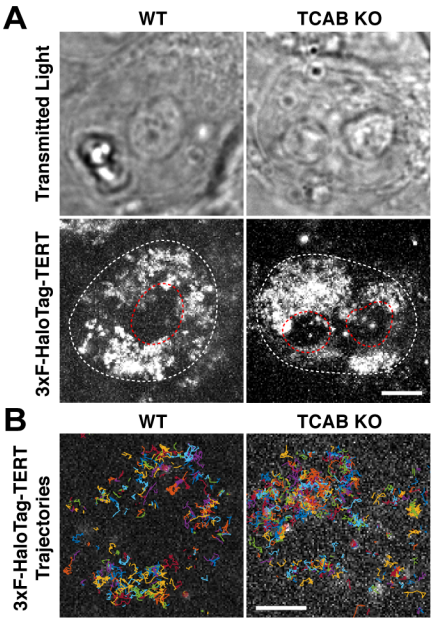

Figure 2. TERT is excluded from nucleoli in control and TCAB1 knock-out cells. (A) Maximum intensity projections of 2000 frames of 3xFLAG-HaloTag (JF646) TERT movies (bottom), demonstrating that the TERT signal does not overlap with the nucleolus detected as circular shape in the transmitted light image in control and TCAB1 knock-out cells (top, red dashed line, scale bar = 2 μm). **(B)** TERT particle trajectories from the cells shown in Fig. 2A, demonstrating that TERT molecules move parallel to or away from the nucleolus when located at the interface between the nucleolus and nucleoplasm.

illumination (Fig. 2A,B, Figure 2 – figure supplement 1, Movie 1,2). TERT trajectories in close proximity to nucleoli revealed that their movement is biased away from the nucleolus, suggesting that TERT is repelled by the nucleolus (Fig. 2B). To exclude the possibility that nucleolar exclusion is a consequence of the 3xFLAG-HaloTag on the N-terminus of TERT used in our experiments, we transiently expressed the 3xFLAG-HaloTag fused to a nuclear localization sequence (NLS) in HeLa cells. Single-molecule imaging demonstrated that the nuclear 3xFLAG-HaloTag signals overlapped with the nucleolus (Figure 2 – figure supplement 1, Movie 3). Similar to the 3xFLAG-HaloTag alone, 3xFLAG-HaloTag-dyskerin also localized to the nucleolus (Figure 2 – figure supplement 1). These results demonstrate that 3xFLAG-HaloTag-TERT is excluded from the nucleolus and that this exclusion is not caused by the 3xFLAG-HaloTag but instead is an intrinsic property of the TERT protein.

TERT and TR localize to distinct nuclear compartments in cells lacking TCAB1

It is well established that telomerase assembly is incomplete in human cancer cells, which leads to substantial pools of TERT and TR that are not assembled into telomerase RNPs (Xi and Cech, 2014). Together with our observation that TERT molecules rarely enter the nucleolus (Schmidt et al., 2016) this suggests that both free TERT and assembled telomerase RNPs do not enter the nucleolus. To test whether, like TR, TERT accumulates in the nucleolus in cells lacking TCAB1, we carried out single-molecule imaging of 3xFLAG-HaloTag-TERT in TCAB1 knock-out cells. Strikingly, TERT localization is unchanged in cells lacking TCAB1 (Fig. 2A,B). This suggests that unlike TR, TERT does not accumulate in nucleoli when TCAB1 is absent.

The experiments described so far demonstrate that TCAB1 is enriched in nucleoli and TERT is excluded from nucleoli in cells lacking TCAB1, but they do not simultaneously detect TERT and TR in the same cell. To overcome this limitation, we over-expressed mCherry-TERT and TR in TCAB1 knock-out cells. In controls, TERT and TR colocalized with dyskerin at telomeres marked by TRF2 (Fig. 3A). In addition, analysis of the TERT signal across the nucleus and nucleolus revealed that TERT was depleted from the nucleolus (Fig. 3B). Importantly, mCherry-dyskerin localized to the nucleolus, demonstrating that the mCherry-tag does not lead to nucleolar exclusion of its fusion partner (Figure 3 – figure supplement 1). In cells lacking TCAB1, mCherry-TERT was diffusely localized in the nucleoplasm, localized to a subset of telomeres, and was depleted from the nucleolus (Fig. 3A,C). Similar to endogenous TR, overexpressed TR was enriched in the nucleolus in TCAB1 knock-out cells (Fig. 3A). In addition, TR was frequently co-localized with telomeres when mCherry-TERT and TR were overexpressed

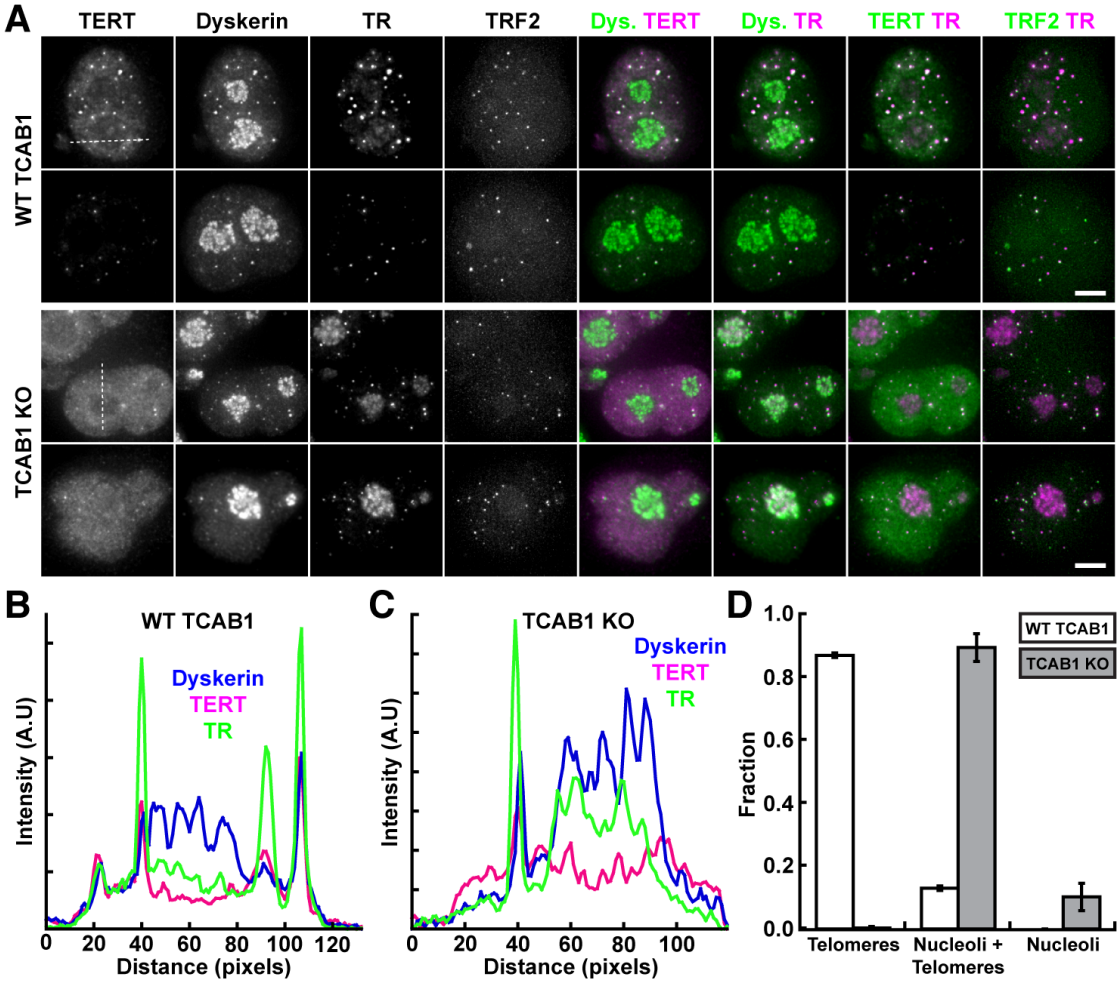

Figure 3. TERT and TR localize to distinct nuclear compartments in TCAB1 knock-out cells. (A) IF-FISH images of control and TCAB1 knock-out HeLa cells (3xFLAG-Halo-TERT, mEOS3.2-TRF2) overexpressing mCherry-TERT and TR (scale bar = 5 μm). Cells were probed with antibodies against dyskerin and mCherry, and FISH probes specific to TR. The intrinsic fluorescence of mEOS3.2-TRF2 was used to detect telomeres. TR and TERT are co-localized at telomeres in control cells. In TCAB1 knock-out cells, TR is enriched in nucleoli, while TERT is depleted from nucleoli in both control and TCAB1 knock-out cells. Both TERT and TR also localize to telomeres in TCAB1 knock-out cells. **(B-C)** Line scans of **(B)** control and **(C)** TCAB1 knock-out cells along the dashed white lines in Fig. 3A, demonstrating the enrichment of TR (green) in nucleoli (blue) in TCAB1 knock-out cells and the depletion of TERT (magenta) from nucleoli in both control and TCAB1 knock-out cells. **(D)** Quantification of the fraction of cells showing TR localization exclusively to telomeres, to telomeres and nucleoli, or only to nucleoli in cells over-expressing mCherry-TERT and TR (3 independent experiments, >100 cells per experiments, mean ± standard deviation).

in cells that lack TCAB1 (Fig. 3A,C-D). Similar TR localization patterns were found when overexpressing untagged TERT and TR (Figure 3 – figure supplement 1) and untagged TERT was excluded from nucleoli, confirming that nucleolar exclusion is an intrinsic property of TERT (Figure 3 – figure supplement 1). Together these results demonstrate

that, when overexpressed in TCAB1 knock-out cells, TR is enriched in nucleoli and TERT is depleted from nucleoli, consistent with a failure of nucleolar TR to assemble with TERT. In addition, our observations suggest that overexpression can partially overcome the sequestration of TR in the nucleolus when TCAB1 is absent, allowing a fraction of TR to bind to TERT and localize to telomeres.

TCAB1 promotes telomerase RNP assembly

Previous studies by other laboratories have concluded that telomerase assembly is unaffected by the absence of TCAB1 and whether TCAB1 is required for telomerase activity is controversial (Chen et al., 2018; Venteicher et al., 2009; Vogan et al., 2016). To assess the role of TCAB1 in telomerase assembly, we immuno-purified endogenous telomerase using a well-established anti-TERT antibody (Cohen et al., 2007). The amount of TERT purified from TCAB1 knock-out cells was reduced compared to control cells (Figure 4A), which likely indicates a lower expression level of TERT in cells lacking TCAB1. In contrast, TR levels were not reduced in cells lacking TCAB1 (Figure 4B). To quantify telomerase assembly, we measured TERT levels by Western blot and determined the amount of TR co-purified using Northern blot (Fig. 4A,B). The fraction of TR associated with TERT was reduced to < 20% in TCAB1 knock-out cells compared to parental controls (Fig. 4C). In addition, the ratio of TR relative to TERT, which is a direct measure of telomerase assembly, was reduced to 20-40% in cells lacking TCAB1 relative to controls (Fig. 4D). This excludes the possibility that the lower amount of TR co-purified with TERT from TCAB1 knock-out cells is a consequence of the reduction of total TERT

immuno-precipitated from these cells (Fig. 4A). These observations strongly suggest that telomerase assembly is defective in cells that lack TCAB1. To further test this hypothesis, we overexpressed TERT and TR in parental and TCAB1 knock-out cells and immuno-purified TERT with the same TERT antibody (Fig. 4E, Figure 4 - figure supplement 1). After overexpression of TERT and TR, the fraction of TR associated with

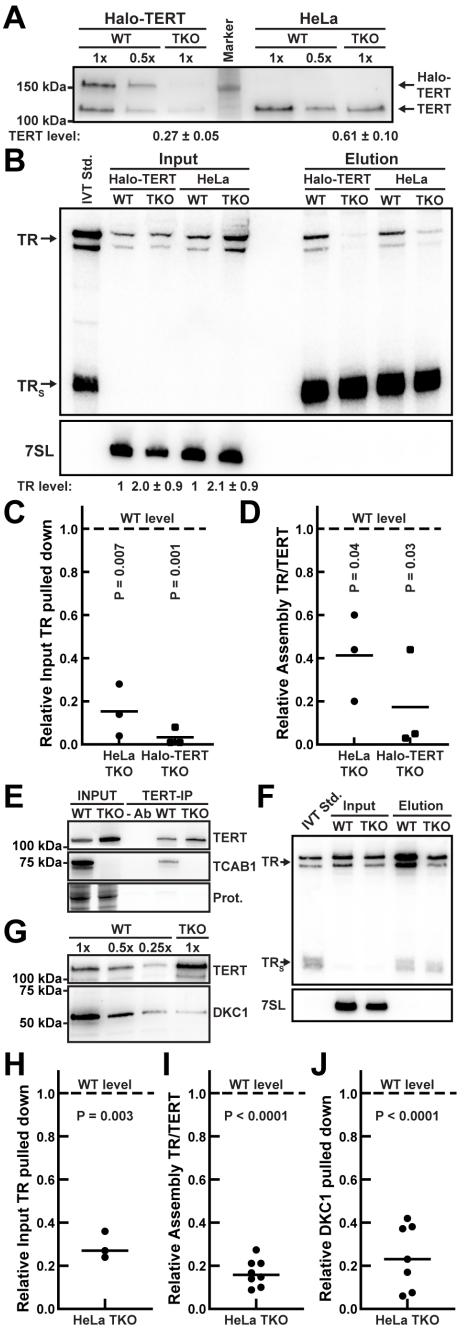

Figure 4. Telomerase Assembly is reduced in the absence of TCAB1. (A) Western blots analyzing endogenous TERT immuno-purification (using a sheep anti-TERT antibody) probed with a rabbit anti-TERT antibody (Abcam). TERT level normalized to WT (n = 3, SD). **(B)** Northern blot of RNA extracted from input and purified endogenous TERT samples probed with radiolabeled DNA oligonucleotides complementary to TR. Standards are *in vitro* transcribed full-length TR and truncated TR_S. TR_S was added to samples prior to RNA extraction as loading and recovery control. Input samples were also probed for 7SL RNA as loading control. Input TR levels relative to WT control normalized to 7SL RNA (n = 3, SD). **(C-D)** Quantification of the amount of **(C)** TR purified relative to input RNA levels, and **(D)** the ratio of TR relative to TERT in telomerase samples purified from TCAB1 knock-out cells compared to controls (n = 3, mean, T-Test). The dashed lines indicate the level in telomerase purified from wild-type TCAB1 cells which was normalized to 1.0. **(E)** Western blots analyzing TERT immuno-purification (using a sheep anti-TERT antibody) from control cells (WT) or TCAB1 knock-out cells (TKO) overexpressing TERT and TR probed with a rabbit anti-TERT antibody (Abcam) and a TCAB1 antibody. **(F)** Northern blot of RNA extracted from input and purified TERT samples from control cells (WT) or TCAB1 knock-out cells (TKO) overexpressing TERT and TR probed with radiolabeled DNA oligonucleotides complementary to TR. Standards are *in vitro* transcribed full-length TR and truncated TR_S. TR_S was added to samples prior to RNA extraction as loading and recovery control. Input samples were also probed for 7SL RNA as loading control. **(G)** Western blots to analyze immuno-purified telomerase RNP composition. A single membrane was cut into two pieces that were probed with TERT and dyskerin antibodies, respectively. **(H-J)** Quantification of the amount of **(H)** TR relative to input TR (n = 3), **(I)** the ratio of TR to TERT (n = 8), and **(J)** dyskerin (n = 7) in TERT purifications from TCAB1 knock-out cells overexpressing TERT and TR compared to parental controls (mean, T-Test). The dashed lines indicate the level in telomerase purified from wild-type TCAB1 cells which was normalized to 1.0.

TERT and the ratio of TR relative to TERT were significantly reduced when telomerase was purified from TCAB1 knock-out cells (Fig. 4E-F ,H-I , Figure 4 - figure supplement 1). Furthermore, the increased amount of telomerase purified after over expression allowed us to assess the amount of dyskerin associated with the telomerase RNP (Fig. 4G). Since TR bridges TERT and dyskerin, dyskerin co-purified with TERT directly reports on the presence of TR. Consistent with the reduction in TR, the amount of dyskerin bound to TERT was also reduced when TERT was purified from cells lacking TCAB1 compared to parental controls (Fig. 4G, H, Figure 4 - figure supplement 1). Importantly, we also confirmed that TCAB1 is absent from telomerase purified from TCAB1 knock-out cells (Fig. 4E, Figure 4 - figure supplement 1). Altogether, these results demonstrate that telomerase assembly is significantly reduced (to ~20-40% of control levels) in the absence of TCAB1 and that overexpression of TERT and TR is not sufficient to overcome this defect in telomerase RNP formation.

TCAB1 is not required for telomerase catalytic activity

To assess whether TCAB1 is required for telomerase catalysis, we first analyzed the enzymatic activity of endogenous telomerase purified from TCAB1 knock-out cells using the direct telomerase extension assays (Fig. 5A,B). Consistent with previous results (Chen et al., 2018), telomerase activity was strongly reduced in the absence of TCAB1 (Fig. 5C). To address whether this reduction in telomerase activity was a consequence of the defect in telomerase assembly observed in TCAB1 knock-out cells, we determined the specific activity of telomerase by dividing the measured activity by the amount of TR

231 present in the respective telomerase sample. Due to the very small amount of TR

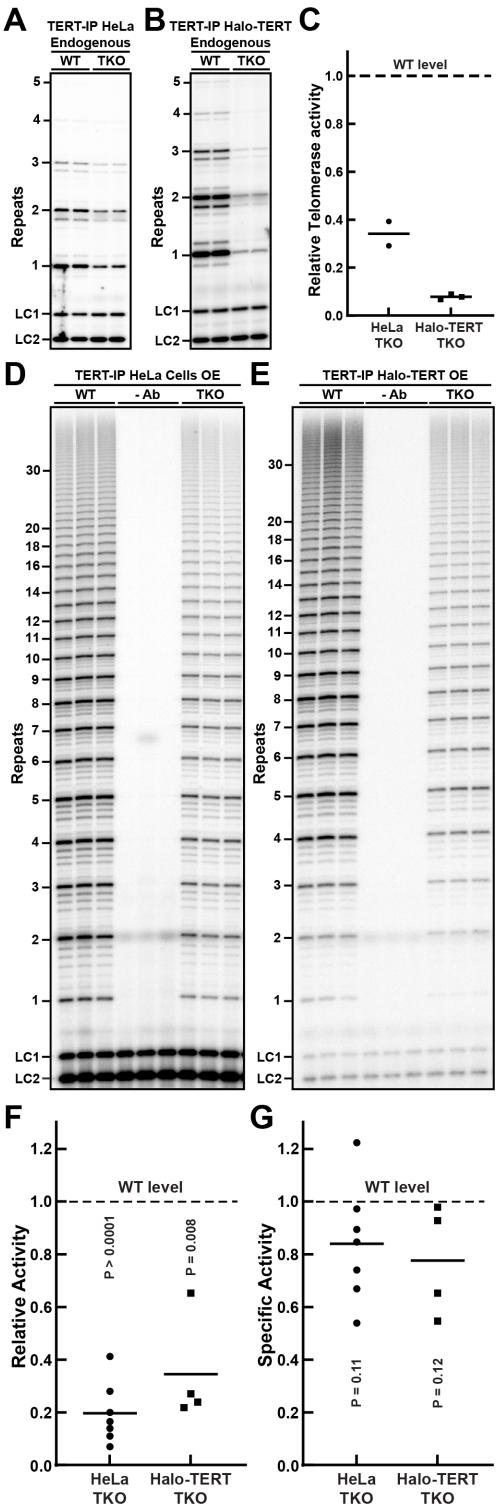

Figure 5. The specific activity of telomerase is unchanged in the absence of TCAB1. (A-B) Direct telomerase extension assay of endogenous telomerase immuno-purified from parental (WT) and TCAB1 knock-out (TKO) **(A)** HeLa and **(B)** Halo-TERT cell lines. Assays were carried out in the presence of 300 mM KCl and limiting amounts of dGTP. LC1 and LC2, radiolabeled DNA oligonucleotide loading controls. **(C)** Quantification of endogenous telomerase activity in samples from TCAB1 knock-out cells relative to parental controls (n = 3, mean). **(D-E)** Direct telomerase extension assay of overexpressed telomerase immuno-purified from parental (WT) and TCAB1 knock-out (TKO) **(D)** HeLa and **(E)** Halo-TERT cell lines. Assays were carried out in the presence of 150 mM KCl and 10 µM dATP, dTTP, and dGTP. LC1 and LC2, radiolabeled DNA oligonucleotide loading controls. In -Ab samples the TERT antibody was omitted during the immuno-purification. **(F)** Quantification of overexpressed telomerase activity in samples from TCAB1 knock-out cells relative to parental controls (n = 4-7, mean). **(G)** Specific activity of overexpressed telomerase purified from TCAB1 knock-out cells relative to parental controls (n = 4-7, mean, T-Test). Specific activity was calculated by dividing the relative activity (see Fig. 5F) by the relative amount of TR present in immuno-purified TERT samples (Fig. 4F). The dashed lines indicate the activity level in telomerase purified from wild-type TCAB1 control cells which was normalized to 1.0.

232

233 detected in endogenous telomerase samples (Fig. 4B-C), quantifying differences in the

234 specific activity of endogenous telomerase was challenging. To overcome this limitation,

we determined the specific activity of telomerase purified from cells overexpressing TERT and TR. Similar to endogenous telomerase, activity of over-expressed telomerase purified from HeLa and Halo-TERT cells lacking TCAB1 was significantly reduced to 24% and 34% compared to controls, respectively (Fig. 5D-F). The specific activity of over-expressed telomerase purified from HeLa and Halo-TERT cells lacking TCAB1 was slightly reduced (84% and 77% relative to control, respectively), but this reduction was not statistically significant (Fig. 5G). Together these observations demonstrate that cellular telomerase activity is reduced in the absence of TCAB1. Importantly, this reduction in catalytic activity corresponds closely to the reduction of telomerase assembly observed in TCAB1 knock-out cells, suggesting that the limited number of telomerase RNPs that form in the absence of TCAB1 are fully active.

TCAB1 is required for telomerase assembly in living cells

The experiments presented thus far demonstrate that telomerase assembly is reduced in the absence of TCAB1 but were carried out in fixed cells or cell lysates. To analyze telomerase assembly in intact cells, we carried out live cell single-molecule imaging of 3xFLAG-HaloTag-TERT and determined the diffusion coefficient of TERT particles (Fig. 6A, Movie 4, Figure 6 – figure supplement 1). The diffusion co-efficient is a measure of the rate of movement of a molecule and depends on the size of the complex it is part of and reports on molecular interactions formed with other sub-cellular structures. Analysis of the diffusion coefficients of TERT trajectories in control cells revealed three distinct populations of TERT particles (Fig. 6B-D). A static population (D_S = 0.03 $\mu m^2/s$, 12%) which likely represents assembled telomerase RNPs bound to telomeres, Cajal bodies or

other cellular structures, a slowly diffusion population (D_{F1} = 0.35 μm^2/s, 28%) and a rapidly diffusing population (D_{F2} = 1.54 μm^2/s, 60%). The slowly diffusing population likely includes assembled telomerase RNPs, while the rapidly diffusing particles represents TERT molecules, which are not assembled with TR (Fig. 6B). Importantly, these diffusion coefficients are largely consistent with our previous results using a distinct analytical method to determine their values (Schmidt et al., 2016). In the absence of TCAB1, the diffusion coefficient of the freely diffusing TERT population was increased (D_{F2} = 1.78 ± 0.04 μm^2/s, mean ± SEM, p = 0.04, Fig. 6C) and the fraction of the TERT populations that includes assembled telomerase RNPs was significantly reduced ($F_{Slow+Static}$ = 29 ± 1%, mean ± SEM, p = 0.02, Fig. 6D). This observation is consistent with our model that in the absence of TCAB1, telomerase assembly is defective. To confirm that the differences in TERT diffusion observed in TCAB1 knock-out cells were a consequences of a reduction in telomerase assembly, we knocked out TR, completely abolishing telomerase assembly. TR knock-out was confirmed by PCR and Sanger sequencing, FISH, and qPCR (Figure 6 – figure supplement 1). Similar to control cells and TCAB1 knock-out cells, TERT was also excluded from nucleoli in cells lacking TR (Figure 6 – figure supplement 1). Strikingly, the diffusion coefficients and the fraction of slow and static TERT particles in cells lacking TR closely resembled those of TCAB1 knock-out cells (Fig. 6A-D, Figure 6 – figure supplement 1, Movie 4-5). It is important to note that, even in TR knock-out cells, 25-30% of TERT particles are slowly diffusing or static (Fig. 6D). Because TR is absent in these cells, the slowly diffusing and static TERT molecules must be the result of interactions of TERT with cellular structures other than Cajal bodies or telomeres. Due to this caveat, we don't believe it is appropriate to use these results to precisely

quantify the degree to which telomerase assembly is affected. The key observation in these experiments is that the changes in TERT diffusion observed in TCAB1 knock-out cells are identical to those observed in TR knock-out cells, which is consistent with a reduction in telomerase assembly when TCAB1 is absent.

To analyze the interaction of TERT with telomeres, we filtered out TERT trajectories that came into proximity with telomeres marked by mEOS3.2-TRF2, as previously described (Schmidt et al., 2016). To assess the interaction of TERT with telomeres, we plotted the step-size vs. the distance from the closest telomere for each step of these trajectories (Figure 6 – figure supplement 2). In control cells, we observed an enrichment of smaller step sizes and particles in close proximity to telomeres, consistent with TERT interactions with the telomere (Figure 6 – figure supplement 2). In contrast, TERT trajectories from TCAB1 knock-out cells lacked this enrichment, and the step size vs. distance from the closest telomere plots were identical to those from TR knock-out cells (Figure 6 – figure supplement 2). In addition, diffusion analysis using SpotOn revealed that the fraction of static TERT particles at telomeres was reduced from 12% in control cells to 4-5% in TCAB1 and TR knock-out cells (Figure 6 – figure supplement 2). These observations indicate that in the absence of either TCAB1 or TR, stable interactions of telomerase with telomeres occur at a lower frequency because they require base pairing of TR with the chromosome end (Schmidt et al., 2018). Together these single-molecule imaging experiments demonstrate that in living cells telomerase assembly is strongly reduced in the absence of TCAB1.

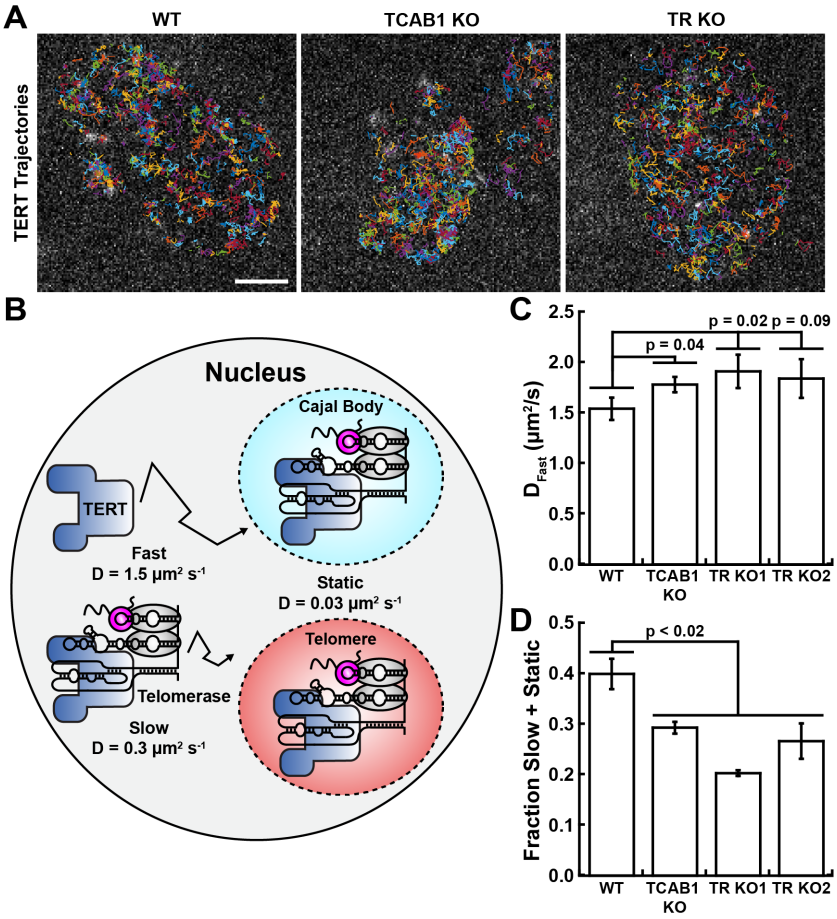

Figure 6. Telomerase assembly is reduced in TCAB1 knock-out cells. (A) TERT particle trajectories from control, TCAB1 knock-out, and TR knock-out cells expressing 3xFLAG-HaloTag TERT (JF646, scale bar = 2 μm). **(B)** Diagram of distinct populations of TERT particles detected in control cells. **(C)** Diffusion coefficient of the rapidly diffusing TERT population in control, TCAB1 knock-out, and TR knock-out cells (3 independent experiments, >15 cells per experiment per cell line, mean ± standard deviation, T-Test, complete data in Fig. S6D). **(D)** Fraction of slow plus static TERT particles in control, TCAB1 knock-out, and TR knock-out cells expressing 3xFLAG-HaloTag TERT (3 independent experiments, >15 cells per experiment per cell line, mean ± standard deviation, T-Test, complete data in Figure 6 – figure supplement 1).

Analysis of nucleolar snoRNP dynamics

The results presented thus far have demonstrated that TR accumulates in nucleoli in the absence of TCAB1 but did not provide any insight into the dynamics of TR association with the nucleolus. Since TR is targeted to nucleoli by dyskerin and other H/ACA RNP components, we used dyskerin as a surrogate for TR and H/ACA snoRNPs in general. We transiently expressed HaloTagged dyskerin in parental HeLa and TCAB1 knock-out

cells and analyzed dyskerin binding to the nucleolus using fluorescence recovery after photobleaching (FRAP). We identified cells with two clearly visible nucleoli, completely photo-bleached the dyskerin signal in one of the nucleoli and quantified the recovery of the fluorescence signal (Fig. 7A, Movies 6-7). The dyskerin signal recovered rapidly ($t_{1/2}$ = 28 s) but only ~65% of the signal was recovered after > 4 minutes (Fig. 7B-D, Movies 6-7). This indicates that there are at least two distinct populations of dyskerin molecules in the nucleolus, a rapidly exchanging population and a static population that does not dissociate from the nucleolus over the time course of this experiment (Fig. 7D). The presence of a mobile dyskerin population was confirmed by analysis of the unbleached nucleolus, which lost fluorescence signal with similar kinetics (Fig. 7A, Figure 7 – figure supplement 1). Importantly, no significant difference in dyskerin dynamics were observed in TCAB1 knock-out cells compared to parental controls (Fig. 7A-D, Figure 7 – figure supplement 1). To further analyze the interaction of dyskerin with the nucleolus, we co-transfected cells with plasmids encoding HaloTagged dyskerin and GFP-NPM1 to mark nucleoli and carried out single-molecule live cell imaging (Fig. 7E, Movie 8). We observed both dynamic and highly static dyskerin molecules in the nucleolus (Fig. 7F, Movie 8). The step size distribution for all tracks was best fit with a three-state model (Figure 7 – figure supplement 1). Like TERT, these three states likely represent free dyskerin, dyskerin that is part of an H/ACA RNP, and dyskerin that is bound to nucleoli or Cajal bodies as part of an H/ACA RNP. To analyze dyskerin binding to the nucleolus we filtered out single-particle trajectories that overlapped with the GFP-NPM1 (Fig. 7F, Figure 7 – figure supplement 1). Consistent with the FRAP analysis, approximately on third of the

dyskerin molecules were statically associated with the nucleolus (Fig. 7F-G, Figure 7 – figure supplement 1). We also confirmed that dyskerin molecules can be associated

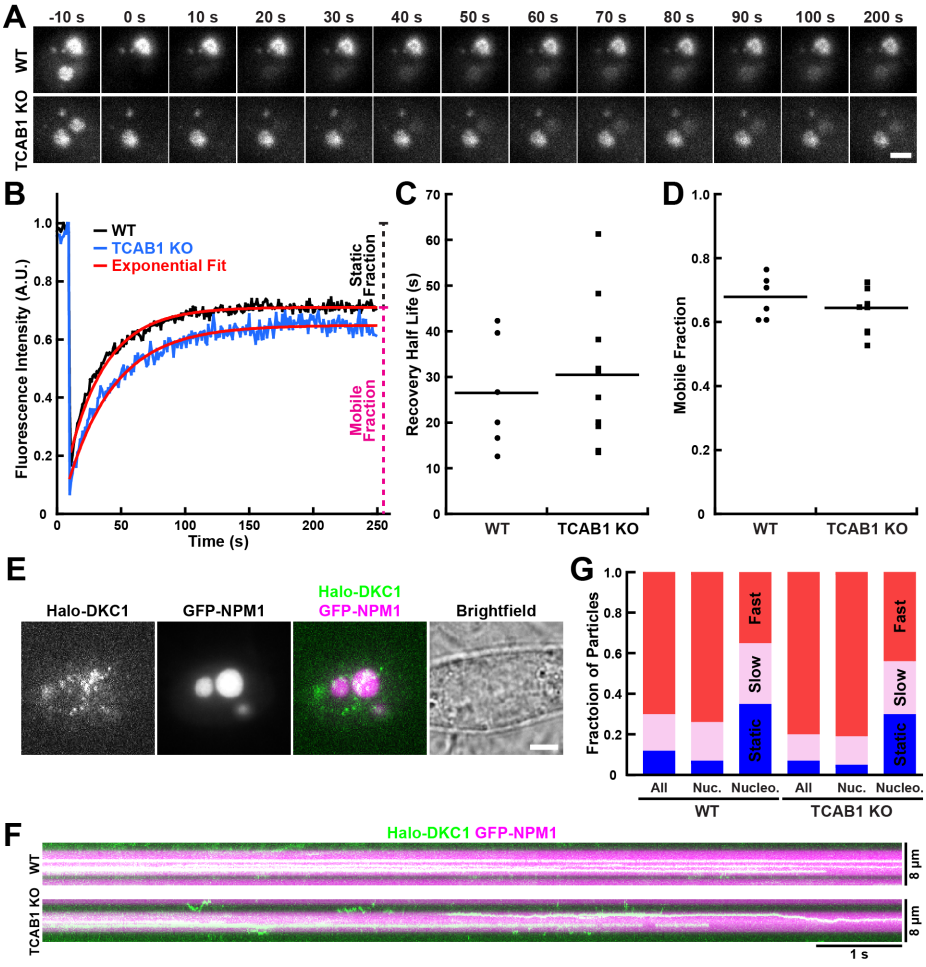

Figure 7. Dyskerin exhibits dynamic and highly static binding to the nucleolus. (A) Images of control and TCAB1 knock-out cells expressing 3xFLAG-HaloTag-dyskerin before and after photobleaching of nucleolar dyskerin (JFX650, scale bar = 5 µm). **(B)** Fluorescence recovery curves of nucleolar dyskerin in control and TCAB1 knock-out cells. Data was fit with a single exponential function. **(C)** Quantification of half-life of fluorescence recovery, calculated from the rate constant of the single exponential fit of the data shown in Fig. 7B (n = 6 and 9, mean). **(D)** Quantification of the mobile fraction of nucleolar dyskerin based on the single exponential fit of the data shown in Fig. 7B (n = 6 and 9, mean). **(E)** Fluorescence images of single 3xFLAG-HaloTag-dyskerin particles, nucleoli marked by GFP-NPM1, and a widefield image of the imaged cell (scale bar = 5 µm). **(F)** Kymographs of nucleolar 3xFLAG-HaloTag-dyskerin particles over time, demonstrating the presence of both static (straight lines) and mobile dyskerin molecules in control and TCAB1 knock-out cells. **(G)** Quantification of the fraction of fast diffusing, slow diffusing, and static 3xFLAG-HaloTag-dyskerin particles in the whole cell (All), nucleoplasm (Nuc.), and nucleolus (Nucleo.), based on Spot-On analysis (data histograms can be found in Figure 8 - figure supplement 1).

335 with the nucleolus for extended periods of time by reducing the imaging rate to 1 frame
336 per second to avoid photobleaching (Figure 7 – figure supplement 1, Movie 9). Similar to
337 the FRAP analysis, no significant difference in dyskerin dynamics were observed in
338 TCAB1 knock-out cells compared to parental controls (Fig. 7E-G, Figure 7 – figure
339 supplement 1). In total, this analysis demonstrates that approximately a third of the
340 dyskerin containing H/ACA RNPs are tightly bound to the nucleolus and do not rapidly
341 exchange with the nucleoplasm.
342
343 **TR is tightly associated with the nucleolus in absence of TCAB1**
344 Our observations demonstrate that dyskerin containing snoRNPs can be either tightly
345 bound to the nucleolus or rapidly exchange with the nucleoplasm. To address whether
346 TR is tightly bound to the nucleolus in the absence of TCAB1 we carried out cellular
347 fractions to isolate nucleoli (Fig. 8, Figure 8 – figure supplement 1). Nucleoli were purified
348 by rupturing isolated nuclei using sonication, followed by centrifugation through a high-
349 density sucrose cushion (Figure 8 – figure supplement 1) (Lam and Lamond, 2006). If TR
350 rapidly dissociated from the nucleolus ($t_{1/2}$ = 28 s), we would expect it to be lost from the
351 nucleolar fraction during centrifugation through the sucrose cushion (10 min). In contrast,
352 if TR was tightly bound to the nucleolus, it should be recovered in the nucleolar fraction.
353 Isolated nucleoli were enriched with the nucleolar protein fribrillarin and the U3 snoRNA,
354 while being depleted of lamin B1 and the 7SK RNA (Fig. 8A,B), which serve as
355 nucleoplasmic markers, demonstrating that we successfully purified nucleoli using this
356 approach. To determine the amount of TR found in the nucleolus and the nucleoplasm,
357 we quantified the level of TR relative to that of the U3 or the 7SK RNA, respectively. In

control cells, the majority of TR was found in the nucleoplasmic fraction, and a small amount of TR was detected in nucleoli (Fig. 8B), consistent with previous work that analyzed TR localization by live cell imaging (Laprade et al., 2020). In contrast, in TCAB1 knock-out cells TR was depleted from the nucleoplasm and enriched in the nucleolus (Fig. 8B,C). To assess the impact that salt has on nucleolar integrity, we supplemented ruptured nuclei with potassium chloride, prior to isolating nucleoli by centrifugation. After exposure to a high salt concentration, fibrillarin and TR were found in the nucleoplasmic fraction instead of the nucleolar pellet (Figure 8 – figure supplement 1), demonstrating that nucleoli are disrupted and TR is released under these conditions. These observations confirm that TR is sequestered in the nucleolus in the absence of TCAB1 and strongly suggest that TR is tightly associated with the nucleolus under these circumstances, preventing it from entering the nucleoplasm to allow telomerase assembly.

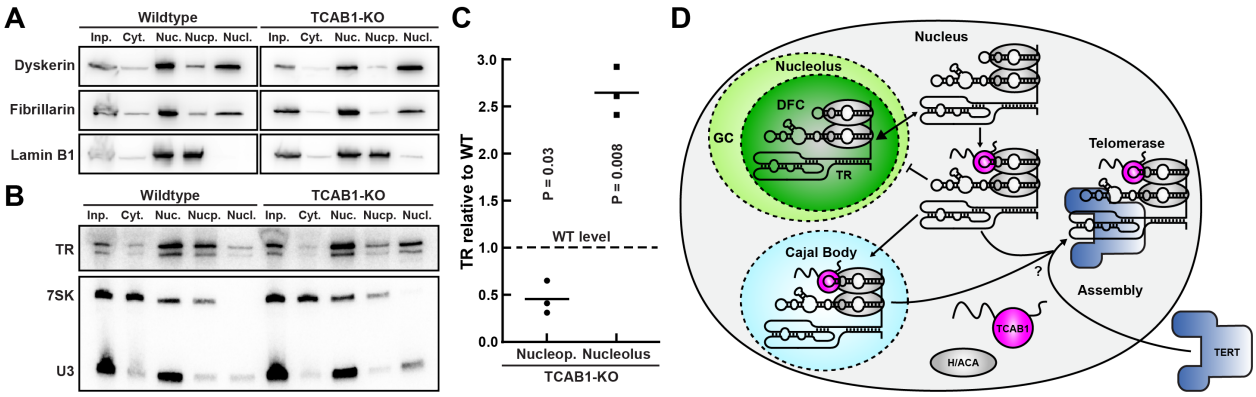

Figure 8. The telomerase RNA is enriched in and tightly bound to the nucleolus. (A) Western blots of samples of cellular fractionation experiments (Input, Cytoplasm, Nucleus, Nucleoplasm, Nucleolus, left to right) from control and TCAB1 knock-out cells. Blots were probed with antibodies against dyskerin, fibrillarin (nucleolar marker), and lamin B1 (nucleoplasmic marker). **(B)** Northern blots of samples of cellular fractionation experiments (Input, Cytoplasm, Nucleus, Nucleoplasm, Nucleolus, left to right) from control and TCAB1 knock-out cells. Blots were first probed with radiolabeled DNA oligonucleotides complementary to TR, followed by probes complementary to the 7SK RNA (nucleoplasmic marker) and the U3 snoRNA (nucleolar marker). **(C)** Quantification of the nucleoplasmic and nucleolar abundance of TR in TCAB1 knock-out cells relative to control cells. Nucleoplasmic TR signal was normalized to the 7SK RNA signal and nucleolar TR signal was normalized to the U3 RNA signal (n = 3, mean, T-Test). **(D)** Model for the regulation of telomerase assembly by TCAB1. In the absence of TCAB1, TR is sequestered in the dense fibrillar component (DFC) of the nucleolus, which is separated from the nucleoplasm by the granular component (GC) of the nucleolus.

Discussion

The experiments described in this study demonstrate that TCAB1 promotes telomerase assembly. In the absence of TCAB1 the telomerase RNA is targeted to the nucleolus via its association with dyskerin and other components of the H/ACA complex. In contrast to TR, TERT cannot enter the nucleolus, preventing its association with TR in cells that lack TCAB1. This demonstrates that nuclear compartmentalization, which is a consequence of nucleolar phase separation, counteracts telomerase assembly. In addition, we demonstrate that sequestration of TR in the phase-separated nucleolus in the absence of TCAB1 can be partially overcome by telomerase overexpression, leading to telomerase assembly and localization to telomeres. This suggests that the nucleolus has a limited capacity to accommodate cellular RNAs and that TCAB1 is not necessary for telomerase recruitment to telomeres. Our analysis of dyskerin bound snoRNP dynamics in nucleoli revealed that a third of these snoRNPs are tightly associated with the nucleolus and that TR is likely included in this fraction. Finally, we demonstrate that while telomerase assembly is limited the specific activity of telomerase is unchanged in the absence of TCAB1, which excludes a role of TCAB1 in telomerase catalytic function. Altogether our work completely reshapes our understanding of the role of TCAB1 in telomerase function in human cells and provides insight into the role phase-separated organelles play in RNP assembly and function.

TCAB1 promotes telomerase assembly

The importance of TCAB1 for telomere maintenance is undisputed (Chen et al., 2018; Venteicher et al., 2009). Knock-out or depletion of TCAB1 results in telomere shortening

(Chen et al., 2018; Venteicher et al., 2009; Vogan et al., 2016). All previous work also concluded that TR is enriched in the nucleolus in the absence of TCAB1 (Chen et al., 2018; Stern et al., 2012; Vogan et al., 2016; Zhong et al., 2011). Finally, all prior studies propose that TCAB1 is not required for telomerase assembly but instead plays a role telomerase trafficking to Cajal bodies and telomeres or is required for telomerase catalysis (Chen et al., 2018; Stern et al., 2012; Venteicher et al., 2009; Vogan et al., 2016; Zhong et al., 2011). In contrast, our results demonstrate that in the absence of TCAB1, TERT and TR are localized to the distinct sub-cellular compartments, the nucleoplasm and the nucleolus, respectively. This spatial separation strongly reduces telomerase assembly, which leads to reduced number of telomerase RNPs per cell and in turn telomere shortening. Importantly, in the absence of TCAB1, telomerase assembly is reduced but not completely abolished. It is likely that TR bound by the H/ACA complex is in an equilibrium between localizing to nucleoplasm and the nucleolus. In the presence of TCAB1, this equilibrium is shifted towards the nucleoplasm because TCAB1 prevents the entry of TR into the nucleolus (Fig. 8D). In contrast, in the absence of TCAB1, the majority of TR is trapped in the nucleolus effectively reducing the amount of TR that is available for assembly with TERT.

The sub-cellular location and order in which telomerase RNP components associate with TR in human cells are largely unknown (Fig. 8D). Our results exclude the possibility that TERT assembles with TR in the nucleolus, and results by others have demonstrated that eliminating Cajal bodies does not impact telomerase activity or telomere maintenance, suggesting that Cajal bodies are not necessary for telomerase assembly (Chen et al., 2018; Vogan et al., 2016). Our single-molecule live cell imaging of

418 TERT has demonstrated that TERT is almost exclusively localized to the nucleus, it is
419 therefore likely that human telomerase assembles in the nucleoplasm. But it cannot be
420 ruled out that in human cells TR is transiently exported to the cytoplasm to assemble with
421 nascent TERT protein, as is the case in *S. cerevisiae* (Gallardo et al., 2008). Interestingly,
422 our results suggest that TERT levels are reduced in the absence of TCAB1. It is possible
423 that TERT protein which fails to assemble with TR is degraded, which could be an
424 important mechanism controlling telomerase abundance.

425 Altogether, our observations support our model that TCAB1 promotes telomerase
426 assembly by counteracting TR accumulation in the nucleolus to facilitate its assembly
427 with TERT. Our model is further supported by work from Vogan *et al.*, which demonstrated
428 that truncated TR (hTRmin) that lacks the H/ACA region and therefore cannot bind
429 dyskerin, accumulates in the nucleoplasm and is excluded from nucleoli (Vogan et al.,
430 2016). Importantly, in cells that express hTRmin, TCAB1 is not required for telomere
431 maintenance (Vogan et al., 2016), consistent with TCAB1 promoting telomerase
432 assembly by preventing TR accumulation in the nucleolus.

433

434 **TCAB1 is not required for telomerase catalysis**

435 Previous work by others has reported conflicting results regarding the role of TCAB1 in
436 telomerase catalysis, ranging from full enzymatic activity in initial reports to substantial
437 activity defects in the most recent study (Chen et al., 2018; Venteicher et al., 2009; Vogan
438 et al., 2016). Importantly, both our work and the only other study that analyzed the role of
439 TCAB1 in telomerase activity using the “gold-standard” direct telomerase extension assay
440 concluded that telomerase activity is significantly reduced in the absence of TCAB1.

While both studies concur on the degree to which telomerase activity is reduced in the absence of TCAB1, the proposed underlying molecular mechanisms differ. Chen *et al*. propose that TCAB1 is required for proper folding of the CR4/CR5 region of the telomerase RNA, which directly associates with TERT, without affecting telomerase assembly (Chen et al., 2018). Recent structural analysis of the telomerase RNP from human cells revealed that TCAB1 is located far away from the CR4/CR5 region of TR (Figure 8 – figure supplement 1) (Ghanim et al., 2021). Although it is possible that telomerase can adopt additional conformations, based on the currently available structural information it is difficult to rationalize a molecular mechanism by which TCAB1 could specifically promote CR4/CR5 folding. In addition, due to the miss-folding of TR telomerase was proposed to adopt a low activity state in the absence of TCAB1. Experimentally such a low activity state would manifest itself as a reduction in the specific activity of telomerase (telomerase activity per assembled telomerase RNP). Our experiments strongly suggest that, while telomerase assembly is reduced in the absence of TCAB1, the limited amount of telomerase that can assemble is close to fully active (i.e. does not have reduced specific activity). One possible explanation for the discrepancies between the work by Chen *et al*. and our study is the methodology used to generate cell lysates. Our results demonstrate that the high salt concentration used by Chen *et al.* to generate nucleolar extracts dissolves nucleoli and releases TR. Consistent with this observation, salt concentrations > 250 mM have been shown to disrupt the phase separation phenomena underlying the formation of the nucleolus (Feric et al., 2016). Solubilization of the nucleolus and release of TR would override the localization of TR and TERT to distinct sub-cellular compartments, and could allow telomerase to assemble

464 in the nuclear extract, while it is limited in cells or cell lysates in which nucleoli remain
465 intact. Altogether, our enzymatic analysis, and the positioning of TCAB1 within the
466 telomerase RNP do not support a role of TCAB1 in TR folding and telomerase catalysis
467 but are fully consistent with TCAB1 promoting telomerase assembly.
468
469 **TCAB1 is not necessary for telomerase recruitment to telomeres**
470 TCAB1 is necessary for the localization of scaRNAs to Cajal bodies and previous work
471 suggested that it is also required for telomerase recruitment to telomeres (Stern et al.,
472 2012; Venteicher et al., 2009). Our observations demonstrate that when TERT and TR
473 are overexpressed in TCAB1 knock-out cells a fraction of TERT can assemble with TR
474 an localize to telomeres. Telomerase recruitment to telomeres requires a direct interaction
475 between TERT and TPP1 (Nandakumar et al., 2012; Schmidt et al., 2014; Zhong et al.,
476 2012), therefore TR that localizes to telomeres must be assembled with TERT. These
477 results are fully consistent with our model that the spatial separation of TR and TERT in
478 the absence of TCAB1 prevents telomerase assembly. When TR is overexpressed the
479 capacity of the nucleolus to sequester TR may be saturated and excess TR can assemble
480 with TERT and localize to telomeres. In addition, our observations suggests that TCAB1
481 is not necessary for telomerase localization to telomeres. Because telomerase was
482 overexpressed in these experiments, we cannot exclude the possibility that TCAB1
483 contributes to telomerase recruitment to telomeres at endogenous expression levels. But
484 the maintenance of telomeres at a short length in TCAB1 knock-out cells suggests that
485 telomerase recruitment to telomeres can occur in the absence of TCAB1.
486

Regulation of RNP assembly by nucleolar phase-separation

In addition to the mechanistic insight into the role of TCAB1 in telomerase function, our results also demonstrate that nucleolar phase separation can effectively regulate telomerase RNP assembly in the nucleus of human cells. How RNA molecules are specifically recruited into, excluded from, or expelled from non-membrane bound organelles is a key unanswered question. One model suggests that gradual replacement of non-specific, multivalent interactions of pre-ribosomal RNAs with nucleolar proteins such as NPM1 and fibrillarin, with specific, high-affinity interactions with ribosomal proteins leads to the ejection of mature ribosomal subunits from the nucleolus (Riback et al., 2020). In this model a key driving force for the retention of RNA in the nucleolus is regions of RNA not yet bound by ribosomal proteins, that are available to interact with nucleolar proteins (Riback et al., 2020). By analogy, this model would explain why TR bound by the H/ACA complex but not associated with TERT would be sequestered in the nucleolus. In addition to the interactions formed by the H/ACA complex with nucleolar proteins and RNA, the regions of TR that are bound by TERT in the context of telomerase (i.e. the pseudoknot, template, and CR4/CR5) would be available to form non-specific, multivalent interactions with nucleolar proteins to strengthen the association of TR with the nucleolus and prevent its release.

TR is a unique among the scaRNAs because it contains the additional domains that associate with TERT. Most other box H/ACA scaRNAs are substantially shorter (<150 nucleotides) than TR (451 nucleotides), and do not contain large regions that are not bound by proteins and could form non-specific interactions with nucleolar proteins. It is therefore possible, that in cells lacking TCAB1, TR is strongly retained in the nucleolus

while other scaRNAs are less tightly bound, because they lack additional interaction sites with nucleolar proteins. Consistent with this hypothesis, we observe multiple populations of dyskerin with distinct binding dynamics in nucleoli. The weakly bound population could include dyskerin bound to scaRNAs, that are not retained in the nucleolus because their RNA targets, which would provide an additional interaction site, are not present in nucleoli. In contrast, dyskerin bound to snoRNAs would strongly associate with the nuceolus because they also bind to their target RNAs. This provides a potential explanation for the phenotypes observed in patients with TCAB1 mutations that suffer from dyskeratosis congenita. The patients have a clear deficiency in telomerase function (Zhong et al., 2011), but no defects in splicing have been reported, which would be the consequence of complete loss of scaRNA function and their critical role in spliceosome maturation.

How TCAB1 binding leads to the exclusion of TR and other scaRNA from the nucleolus remains a key unanswered question. TCAB1 interacts with a very short sequence motif in TR, which is far removed from the TR regions that associate with TERT (Fig. 8 – Figure supplement 1) (Ghanim et al., 2021). It is therefore unlikely that TCAB1 binding leads to expulsion of TR from the nucleolus by reducing the number of non-specific, multivalent interactions TR can form with nucleolar proteins. As outlined above, we believe that TCAB1 prevents localization of scaRNAs to the nucleolus, rather than extracting scaRNAs that are already localized to the DFC. One potential explanation is that TCAB1 counteracts scaRNA recruitment to the nucleolus by inhibiting the nucleolar localization signals within dyskerin (Heiss et al., 1999). Dissecting the molecular mechanism by which TCAB1 leads to exclusion of TR from the nucleolus in future studies

533 will undoubtably shed light on the fundamental principles RNP recruitment to non-
534 membrane bound organelles and its physiological role in cell biology.
535

Acknowledgements

We would like to thank members of the Schmidt lab and J. Nandakumar for discussions and critical reading of the manuscript and Luke Lavis (HHMI Janelia Research Campus) for providing HaloTag dyes. This work was supported by grants from the NIH (R00 GM120386, R01GM141354) to J.C.S.. J.C.S. was a Damon Runyon Dale F. Frey Scientist supported (in part) by the Damon Runyon Cancer Research Foundation (DFS-24-17). S.B.C. acknowledges sustained support from the Ernest & Piroska Major Foundation.

Author contributions

B.S.A.-M. carried out IF-FISH experiments, telomerase purifications, cellular fractionations, analyzed telomerase assembly, generated mCherry- and 3xFLAG-HaloTag-dyskerin plasmids, determined their sub-cellular localization, and edited the manuscript. G.I.P. maintained cell lines, established TCAB1 and TR knock-out cell lines and carried out IF-FISH experiments. K.A.-B. assisted in establishing the TR knock-out cell line and carried out characterization of the TR knock-out cells. S.B.C. purified and characterized the anti-TERT sheep antibody. L.H. and K.Y. characterized TCAB1 knock-out clones using Southern blots. J.C.S. carried out all other experiments, designed the research, analyzed data, and wrote the manuscript.

Competing interests

The authors declare no competing interests.

Materials and Methods

Cell Lines and Tissue Culture

All cell lines were based on HeLa-EM2-11ht (Weidenfeld et al., 2009) and were cultured in Dulbecco's Modified Eagle Medium including L-glutamine (Gibco) supplemented with 10% fetal bovine serum, 100 units/ml penicillin and 100 µg/ml streptomycin at 37°C with 5% CO_2. Live cell imaging was carried out using CO_2 independent media supplemented with 2 mM GlutaMAX (Life Technologies), 10% fetal bovine serum, 100 units/ml penicillin and 100 µg/ml streptomycin at 37°C with 5% CO_2. For single-molecule imaging of HaloTag-TERT cell were cultured in homemade imaging dishes made by gluing 22x22 mm Nexterion coverslips (170 ± 5 µm, Schott) onto the bottom of plastic 3.5 x 1.0 cm cell culture dishes with a hole in the middle using an epoxy adhesive. Prior to chamber assembly the coverslips were washed with 1 M KOH and 100% for 30 min each in a sonicating water bath. To enrich for cells in S-phase for live cell imaging experiments, cultures we treated with complete media including 2 mM thymidine for a minimum of 16 hours. Cells were released 2 hours prior to imaging by replacing the thymidine containing media with fresh media without thymidine. Puromycin selection was carried out at a concentration of 1 µg/ml.

Plasmid Construction and Genome Editing

All plasmids were generated by Gibson assembly (NEB) using standard protocols or by inverse PCR. All plasmids will be made available on Addgene. All Cas9 and sgRNA expression plasmids were based on pX330 (Cong et al., 2013). The homologous recombination donor for the TR knock-out was generated by assembling the genomic

sequences immediately upstream and downstream (~500 bp each) of the TR sequence flanking a puromycin resistance cassette into HpaI linearized pFastBac. The 3xFLAG-HaloTag-NLS plasmids was generated by adding a 3xFLAG-tag to a previously described HaloTag-NLS plasmid (a kind gift from X. Darzacq and A. Hansen) (Hansen et al., 2018). The 3xFLAG-HaloTag-dyskerin plasmid was generated by replacing TERT in our previously described 3xFLAG-HaloTag-TERT expression plasmid with the dyskerin coding sequence (Schmidt et al., 2016). The mCherry-dyskerin plasmid was generated by replacing TERT in our previously described mCherry-TERT expression plasmid with the dyskerin coding sequence (Schmidt et al., 2014). Unless otherwise stated transfections were carried out using Lipfectamine 2000 (Invitrogen) using the manufacturer's instructions. For FRAP analysis of dyskerin $1x10^6$ HeLa cells were transfected with 1 µg of 3xFLAG-HaloTag-dyskerin plasmid using the Lonza 4D-Nucleofector with the SE Cell Line 4D-Nucleofector X kit (Cat. V4XC-1012) and program CN-114. For single-molecule imaging of dyskerin 1 µg of a GFP-NPM1 plasmid was included in addition to the 1 µg of 3xFLAG-HaloTag-dyskerin plasmid. GFP-NPM1 WT was a gift from Xin Wang (Addgene plasmid #17578; http://n2t.net/addgene:17578; RRID:Addgene_17578) (Wang et al., 2005). TCAB1 was knocked-out using a single sgRNA or two separate sgRNA and Cas9 encoding plasmids that were transfected alongside a GFP-expression plasmid. 24 hours after transfection single-cell clones were sorted using the GFP signal. TCAB1 knock-out clones were screened by PCR and confirmed by western blot, Southern Blotting of the *TCAB1* locus and immunofluorescence imaging. TR was knocked out by transfecting two sgRNA plasmids and a homologous recombination donor plasmid. 48 hours after transfection puromycin

604 selection was initiated and 1 week after the initiation of selection single-cell clones were
605 generated by dilution into 96-well plates. TR knock-out was confirmed using PCR and
606 Sanger sequencing, fluorescence *in situ* hybridization, and RT-qPCR.
607
608 **Immunofluorescence and Fluorescence *In Situ* Hybridization Imaging**
609 Fixed cell immunofluorescence imaging and fluorescence *in situ* hybridization was carried
610 out as previously described (Schmidt et al., 2014). Briefly, cells grown on coverslips were
611 fixed in PBS supplemented with 4% formaldehyde. When using the HaloTag for
612 fluorescence detection cells were incubated with 100 nM of JF646 HaloTag-ligand for 30
613 min prior to fixation. Unincorporated ligand was removed by 3 washes with complete
614 media followed by placing the cells back in the incubator for 10 min to let additional dye
615 leak out of the cells. mEOS3.2-TRF2 was detected using the intrinsic fluorescence of
616 green form of mEOS3.2. After removing the fixation solution using 2 PBS washes,
617 coverslips were transferred into aluminum foil covered humidity chambers with a parafilm
618 layer and rinsed with 1 ml of PBS with 0.2% Triton X-100. Cells were than incubated in
619 blocking buffer (PBS, 0.2% Triton X-100, 3% BSA) for 30 minutes, followed by incubation
620 with primary antibodies diluted in blocking buffer for 1 hour. All primary antibodies were
621 used at a concentration of 1 µg/ml. After three washes with PBS + 0.2% Triton X-100,
622 coverslips were incubated with secondary antibodies diluted in PBS + 0.2% Triton X-100
623 for 1 hour. All secondary antibodies were used at a concentration of 4 µg/ml. Cells were
624 washed three times PBS + 0.2% Triton X-100 prior to a second fixation with PBS + 4%
625 formaldehyde. In cases where nuclear staining was used the first of the three washing
626 steps also included 0.1 µg/ml HOECHST. After the second fixation steps coverslips were

dehydrates in three steps with ethanol (70%, 95%, 100%), re-hydrated in 2xSSC + 50% formamide, blocked for 1 hour in hybridization buffer (100 mg/ml dextran sulfate, 0.125 mg/ml *E. coli* tRNA, 1 mg/ml nuclease free BSA, 0.5 mg/ml salmon sperm DNA, 1 mM vanadyl ribonucleoside complexes, 50% formamide, 2xSSC) at 37°C, before incubating the coverslips in hybridization buffer supplemented with three TR probes (30 ng per coverslip,
/5Cy5/GCTGACATTTTTTGTTTGCTCTAGAATGAACGGTGGAAGGCGGCAGGCCGAGGCTT,
/5Cy5/CTCCGTTCCTCTTCCTGCGGCCTGAAAGGCCTGAACCTCGCCCTCGCCCCCGAGAG,
/5Cy5/ATGTGTGAGCCGAGTCCTGGGTGCACGTCCCACAGCTCAGGGAATCGCGCCGCGCGC) over night at 37°C. Probe sequences were previously described (Tomlinson et al., 2006). After hybridization coverslips were washes twice for 30 minutes in 2xSSC + 50% formamide and then mounted on slides using ProLong Antifade Diamond mounting media (Life Technologies). Microscopy was carried out using a DeltaVision Elite microscope using a 60x PlanApo objective (1.42 NA) and a pco.edge sCMOS camera. We acquired 20 Z-sections spaced by 0.2 µm, followed by image deconvolution and maximum intensity projection of the sections using the DeltaVision Softworx software.

Single-Molecule Live Cell Imaging

Live cell single-molecule imaging was carried out on a Olympus IX83 inverted microscope equipped with a 4-line cellTIRF illuminator (405 nm, 488 nm, 561 nm, 640 nm lasers), an Excelitas X-Cite TURBO LED light source, a Olympus UAPO 100x TIRF objective (1.49

NA), a CAIRN TwinCam beamsplitter, 2 Andor iXon 897 Ultra EMCCD cameras, a cellFRAP with a 100 mW 405 nm laser, and a blacked-out environmental control enclosure. The microscope was operated using the Olympus cellSense software. 3xFLAG-HaloTag-TERT was labeled for 2 min in complete media supplemented with 100 nM JF646-HaloTag ligand (Grimm et al., 2015). After removing the HaloTag-ligand with three washes in complete media, cells were placed back in the incubator for 10 min to allow unincorporated dye to leak out of the cells. Cells were then transferred into CO_2 independent media and put on the microscope which was heated to 37°C. Single-molecule imaging was carried out at 50 or 100 frames per second using highly inclined laminated optical sheet illumination (Tokunaga et al., 2008). Movies were typically 20 seconds in length (2000 frames) and were followed by a transmitted light acquisition to visualize overall cell morphology.

For single-molecule imaging of 3xFLAG-HaloTag-Dyskerin, cells were labeled with 100 pM of JFX650-HaloTag Ligand (Grimm et al., 2020) for 1 min. Imaging was carried out at 100 frames per second and images of GFP-NPM1 were taken before and after single-molecule movies of dyskerin to assure the position of the nucleolus had not shifted.

RT-qPCR

RNA samples for RT-qPCR analysis were generated by using RNeasy Mini kits (Qiagen) using ~2 million cells as starting material. Reverse transcription was carried out using random hexamer primers and SuperScript III reverse transcriptase (Invitrogen) according to the manufacturer's instructions. qPCR was carried out using the Maxima SYBR Green qPCR master mix (Thermo Scientific) using primers for GAPDH and TR according to the

673 manufacturer's instructions. All qPCR reactions were carried out in triplicates and three
674 independent biological replicates were analyzed.
675
676 **Southern Blotting**
677 Southern blotting was carried out using standard protocols (Southern, 2006). Briefly,
678 genomic DNA generated by phenol-chloroform extraction after cell lysis using TE
679 supplemented with 0.5% SDS and 0.1 mg/ml Proteinase K, was digested with BamHI
680 (generating a 1394 bp fragment spanning exons 1-3 of the *TCAB1* locus) and separated
681 on a 0.8% agarose gel. The DNA was then transferred on a Hybond-N+ nylon membrane
682 using capillary transfer. The *TCAB1* locus was detected using radioactive probes (alpha-
683 ^{32}P-dCTP) generated by randomly primed DNA synthesis using an 800 bp PCR product
684 overlapping with the 1394 bp restriction fragment as a template and Klenow polymerase
685 (NEB). Telomeric restriction fragment analysis was carried out as previously described
686 (Nandakumar et al., 2012).
687
688 **Western Blotting**
689 Mini-PROTEAN TGX stain-free gels (Bio-Rad) were used for SDS-PAGE. Total protein
690 was detected using a ChemiDoc MP (Bio-Rad) after a 45 second UV activation. Western
691 transfer was carried out using the Trans-Blot Turbo transfer system (Bio-Rad) according
692 to the manufacturer's instructions using the mixed molecular weight transfer setting.
693 Immuno-blotting was carried out using standard protocols. The C-terminal TCAB1
694 antibody (Proteintech, 14761-1-AP) was used at a 1:2000 dilution, the N-terminal TCAB1
695 antibody (Novus Biologicals, NB100-68252) was used at a 1:1000 dilution, the TERT

antibody (Abcam, ab32020) was used at a 1:4000 dilution, the dyskerin antibody (Santa Cruz Biotech, sc-373956) was used at a 1:200 dilution, the fibrillarin antibody was used at a 1:2000 dilution (Novus Biologicals, NB300-269), and the lamin B1 antibody was used a 1:2000 dilution. Secondary antibodies were used at a 1:5000 dilution.

Northen Blotting

RNA was extracted from cell lysates, cellular fractions, and purified telomerase samples using the RNeasy Mini kit (Qiagen) and eluted in 30 ul of RNase free water. Purified telomerase samples were supplemented with 10 ng of a loading and recovery control prior to RNA extraction (*in vitro* transcribed TR 34-328). 15 ul of eluted RNA was mixed with 15 ul of 2x formamide loading buffer (0.1XTBE, 25 mM EDTA, 0.1% bromophenol blue, 0.1% xylene cyanol, 93% formamide) and heated to 60 °C for 5 min. Samples were separated on a 6% TBE, 7M Urea, polyacrylamide gel (Life Technologies), and transferred to a Hybond N+ membrane (Cytiva) using a wet-blotting apparatus in 1x TBE for 2 hours at 0.5 A of constant current in the cold room. After transfer, membranes were UV-crosslinked, and pre-hybridized in Church buffer for 2 hours at 50 °C. Three DNA oligos complementary to TR (GACTCGCTCCGTTCCTCTTC, GCTCTAGAATGAACGGTGGAA, CCTGAAAGGCCTGAACCTC, CGCCTACGCCCTTCTCAGT, ATGTGTGAGCCGAGTCCTG), 7SL (GCGGACACCCGATCGGCATAGC), U3 (GCCGGCTTCACGCTCAGGAGAAAACGCTACCTCTCTTCCTCGTGG), and 7SK (GTGTCTGGAGTCTTGGAAGC) were radioactively labeled using T4 PNK (NEB) and ~10x10^6 cpm of each probe were added to the membrane. Hybridization was carried out

719 at 50 °C overnight. Membranes were washed three times with 2xSSC, 0.1% SDS prior to
720 exposure to a storage phosphorescence screen (Cytiva) which was then imaged on an
721 Amersham Typhoon IP phosphoimager (Cytiva).
722
723 **Telomerase Expression and Purification**
724 Cell lines were transfected in 15 cm tissue culture plates at ~90% confluency (~25-30x10^6
725 cells) using 7.5 µg of TERT plasmid, 30 µg of TR plasmid and 75 µl of Lipofectamine 2000
726 in 1875 ul of Opti-MEM (Cristofari and Lingner, 2006). Transfected cells were split to three
727 15 cm dishes 24 hours after transfection. 48 hours after transfection cells were counted,
728 harvested, and snap frozen in liquid nitrogen. Cells were lysed in 1 ml of CHAPS lysis
729 buffer supplemented with 5 µl of RiboLock RNase inhibitor (10 mM TRIS pH 7.5, 1 mM
730 $MgCl_2$, 1 mM EGTA pH 8.0, 0.5% CHAPS, 10% glycerol) per 100x10^6 cells and rotated
731 at 4 °C for 30 min. Lysates were cleared in a table-top centrifuge at 21,000xg for 15 min
732 at 4 °C. Identical cell equivalents were used for all samples. 45 µg of anti-TERT antibody
733 was added per ml of cleared lysate and samples were rotated for 1 hour at 4 °C. Lysates
734 were then added to 100 µl of protein G agarose and rotated for 1 hour at 4 °C. The resin
735 was spun down at 1000xg and washed four times with 1 ml of Buffer W (20 mM HEPES
736 pH 7.9, 300 mM KCl, 2 mM $MgCl_2$, 1 mM EDTA, 1 mM DTT, 1 mM PMSF, 0.1% Triton X-
737 100, 10% glycerol). TERT was eluted in 100 µl of Buffer W supplemented with 5 µl of 1
738 mM TERT peptide by rotating for 30 min at room temperature.
739
740 **Telomerase Activity Assays**

Telomerase assays were carried out in 20 µl of reaction buffer (50 mM TRIS pH 8.0, 150 mM KCl, 1 mM MgCl2, 2 mM DTT, 100 nM TTAGGGTTAGGGTTAGG oligo, 10 µM dATP, 10 µM dGTP, 10 µM dTTP, 0.165 µM dGTP [α-32P] 3000 Ci/mmol) including 2 µl of purified telomerase for 1 hour at 30 °C. Telomerase was incubated with the substrate oligo for 15 min at room temperature, prior to initiating the reaction by addition of dNTPs. Reactions were stopped by adding 100 µl of 3.6 M of ammonium acetate supplemented with 20 µg of glycogen and 32P 5'-end labeled loading control oligos (TTAGGGTTAGGGTTAGGG, TTAGGGTTAGGGTTAG). Reaction products were precipitated using 500 µl of ice-cold ethanol and stored at -20 °C over-night. Reaction products were spun down in a table-top centrifuge at max speed for 30 min at 4 °C, washed with 500 µl of 70% ethanol, and spun down again speed for 30 min at 4 °C. The 70% ethanol was decanted, and the reaction products were dried in an Eppendorf vacuum concentrator at 45 °C. Reaction products were resuspended in 20 µl of loading buffer (0.05XTBE, 25 mM EDTA, 0.05% bromophenol blue, 0.05% xylene cyanol, 46.5% formamide) and incubated at 95 °C for 5 min. 10 µl of each sample was separated on a 12% polyacrylamide, 7 M urea sequencing gel pre-run for 45 min at 90W. Gels were dried and exposed to a storage phosphorescence screen (Cytiva) and imaged on an Amersham Typhoon IP phosphoimager (Cytiva).

Nucleolar Isolation

Cellular fractionation was carried out using a as previously described (Lam and Lamond, 2006). All procedures were carried out on ice and centrifugations at 4 °C. Approximately $1x10^6$ million cells were harvested by trypsinization, washed with PBS, followed

764 by incubation in a hypotonic buffer (10 mM HEPES pH 7.9, 10 mM KCl, 1.5 mM $MgCl_2$,
765 0.5 mM DTT) to swell the cells. A small fraction of the swollen cells was collected as input
766 sample. Swollen cells were then ruptured using pre-cooled dounce homogenizer and the
767 tight pestle (VWR Cat. 62400-595). The ruptured cells were centrifuged at 218xg for 5
768 min to pellet nuclei. Nuclei where then resuspended in buffer S1 (0.25 M sucrose, 10 mM
769 $MgCl_2$), layered on top of buffer S2 (0.35 M sucrose, 0.5 mM $MgCl_2$) in a 15 ml conical
770 tube, and centrifuged at 1430xg in a swinging bucket rotor for 5 min to further purify nuclei.
771 Nuclei were resuspended in buffer S2 and sonicated on ice for 10 seconds at 30% power
772 (Fisherbrand Model 505, 500W). The sonicated nuclei were then layered on top of buffer
773 S3 (0.88 M sucrose, 0.5 mM $MgCl_2$) and centrifuged at 3000xg in a swinging bucket rotor
774 for 5 min to further purify nucleoli. The nucleolar pellet was suspended in buffer S2 and
775 centrifuged a final time at 1430xg to yield a highly purified nucleolar pellet, which was
776 resuspended in buffer S2. Equal fractions of input, cytoplasm, nuclei, nucleoplasm, and
777 nucleoli samples were collected and analyzed by western and northern blots. To test the
778 impact of salt concentration on the integrity of nucleoli, nuclei ruptured by sonication were
779 mixed 1:1 with buffer S2 containing 40 mM HEPES pH7.9 with and without 715 mM KCl,
780 prior layering the solution on top of buffer S3.
781
782 **Single-Particle Tracking**
783 Single-particle tracking was carried out in MATLAB 2019a using a batch parallel-
784 processing version of SLIMfast modified to allow the input of TIFF files (kindly provided
785 by Xavier Darzacq and Anders Hansen) (Hansen et al., 2018), an implementation of the
786 Multiple-Target-Tracing algorithm (Sergé et al., 2008), with the following settings:

Exposure Time = 10 ms, NA = 1.49, Pixel Size = 0.16 µm, Emission Wavelength = 664 nm, D_{max} = 5 µm^2/s, Number of gaps allowed = 2, Localization Error = 10^{-5}, Deflation Loops = 0. Diffusion coefficients and the fraction of molecules in each distinct particle population were determined using the MATLAB version of the Spot-On tool (kindly provided by Xavier Darzacq and Anders Hansen) (Hansen et al., 2018) with the following settings: TimeGap = 10 ms or 20 ms, dZ = 0.700 µm, GapsAllowed = 2, TimePoints = 8, JumpsToConsider = 4, BinWidth = 0.01 µm, PDF-fitting, D_Free1_3State = [1 25], D_Free2_3State = [0.1 1], D_Bound_3State = [0.0001 0.1]. For all experiments we carried out 3 independent biological replicates with at least 15 cells for each cell line. The statistical significance of differences in particle fractions and diffusion coefficients were assessed using a two-tailed T-Test.

For the analysis of dyskerin trajectories a mask of the nucleolus was generated manually using the threshold function in FIJI. Dyskerin trajectories whose coordinates overlapped with the nucleolar mask for a single frame were designated as nucleolar trajectories. The remaining trajectories were designated nuclear trajectories. All data sets were then analyzed using Spot-On as described above.

Fluorescence recovery after photobleaching

Fluorescence recovery experiments (FRAP) we carried out using the same Olympus microscope used for single-molecule imaging. Cells were stained for 10 min with 100 nM JFX650-HaloTag ligand in complete media. After removing the HaloTag-ligand with three washes in complete media, cells were placed back in the incubator for 10 min to allow unincorporated dye to leak out of the cells. Cells were then transferred into CO_2

independent media and put on the microscope which was heated to 37°C. We identified cells with two clearly visible nucleoli and bleached one of them by placing three diffraction limited bleach spots within the nucleolar 3xFLAG-HaloTag-dyskerin signal. Each spot was bleached for 100 ms at 50% laser power, which lead to complete loss of the fluorescence within the nucleolus. Cells were imaged prior to and after bleaching at 1 frame per second using the Excelitas X-cite TURBO LED light source and the 100x objective. Photobleaching due to LED exposure was negligible. To quantify FRAP we first drift corrected the movie using NanoJ (Laine et al., 2019), we then placed a region of interest (ROI) within the nucleolus and quantified mean intensity within the ROI over time. Background signal was determined in an area of the field of view that was not covered by a cell and subtracted from the nucleolar ROI. In addition, the mean fluorescence after the bleaching pulse was divided by the fraction of total cellular fluorescence remaining after the bleaching pulse. Because the laser pulse bleaches a significant amount of total cellular fluorescence (typically 20-40%), this normalization is critical to determine the maximal amount of fluorescence recovery possible. For example, if 30% of total cellular fluorescence is lost due to the bleaching pulse, the maximal fraction of pre-bleach fluorescence than can theoretically be recovered is 70%. The recovery data was then fit using a single exponential function ($1-A*e^{-kt}+C$), where k corresponds to the rate constant and C to the fraction of the initial signal that is not recovered (i.e. the static fraction).

Quantification of Fixed Cell Imaging

For the quantification of cellular TR distribution in control and TCAB1 knock-out cells we assigned cells into one of three categories: Cells with TR only at telomeres, Cells with TR

only in nucleoli, Cells with TR at telomeres and in nucleoli. We carried out 3 independent biological replicates and counted a minimum of 100 cells for control and TCAB1 knock-out cells.

Quantification of RT-qPCR data

RT-qPCR experiments were carried out in triplicate and the TR Ct value was normalized to the GAPDG Ct value. The mean ΔCt (Ct of TR – Ct of GAPDH) value from three independent experiments and the corresponding standard deviation were plotted.

Quantification of Western Blots, Northern Blots, and Telomerase Activity Assays

Gel images from Western Blots, Northern Blots, and Telomerase Activity Assays were analyzed using ImageQuant TL 8.2. To quantify TR levels in Northern blots the TR band intensity was normalized to the loading and recovery control signal added to the RNA sample prior to RNA purification. To quantify telomerase activity the whole lane intensity starting at repeat 1 was determined and divided by the sum of the loading control signals. Telomerase processivity was calculated by dividing product intensity > 7 repeats by the total signal in the respective lane. The statistical significance of the observed differences was calculated using a two-tailed T-test using a minimum of three biological replicates. Each biological replicate (independent telomerase expression and purification) was analyzed in technical triplicate.

855 **References**

856
857

858 Angrisani A, Vicidomini R, Turano M, Furia M. 2014. Human dyskerin: beyond
859 telomeres. *Biol Chem* **395**:593–610. doi:10.1515/hsz-2013-0287

860 Armanios M, Blackburn EH. 2012. The telomere syndromes. *Nat Rev Genet* **13**:693
861 704. doi:10.1038/nrg3246

862 Chen L, Roake CM, Freund A, Batista PJ, Tian S, Yin YA, Gajera CR, Lin S, Lee B,
863 Pech MF, Venteicher AS, Das R, Chang HY, Artandi SE. 2018. An Activity Switch in
864 Human Telomerase Based on RNA Conformation and Shaped by TCAB1. *Cell* **174**.
865 doi:10.1016/j.cell.2018.04.039

866 Cohen SB, Graham ME, Lovrecz GO, Bache N, Robinson PJ, Reddel RR. 2007. Protein
867 Composition of Catalytically Active Human Telomerase from Immortal Cells. *Science*
868 **315**:1850–1853. doi:10.1126/science.1138596

869 Cong L, Ran FA, Cox D, Lin S, Barretto R, Habib N, Hsu PD, Wu X, Jiang W, Marraffini
870 LA, Zhang F. 2013. Multiplex Genome Engineering Using CRISPR/Cas Systems.
871 *Science* **339**:819–823. doi:10.1126/science.1231143

872 Cristofari G, Lingner J. 2006. Telomere length homeostasis requires that telomerase
873 levels are limiting. *Embo J* **25**:565 574. doi:10.1038/sj.emboj.7600952

874 Feric M, Vaidya N, Harmon TS, Mitrea DM, Zhu L, Richardson TM, Kriwacki RW, Pappu
875 RV, Brangwynne CP. 2016. Coexisting Liquid Phases Underlie Nucleolar
876 Subcompartments. *Cell* **165**:1686 1697. doi:10.1016/j.cell.2016.04.047

877 Freund A, Zhong FL, Venteicher AS, Meng Z, Veenstra TD, Frydman J, Artandi SE.
878 2014. Proteostatic Control of Telomerase Function through TRiC-Mediated Folding of
879 TCAB1. *Cell* **159**:1389 1403. doi:10.1016/j.cell.2014.10.059

880 Gallardo F, Olivier C, Dandjinou AT, Wellinger RJ, Chartrand P. 2008. TLC1 RNA
881 nucleo-cytoplasmic trafficking links telomerase biogenesis to its recruitment to
882 telomeres. *Embo J* **27**:748 757. doi:10.1038/emboj.2008.21

883 Ghanim GE, Fountain AJ, Roon A-MM van, Rangan R, Das R, Collins K, Nguyen THD.
884 2021. Structure of human telomerase holoenzyme with bound telomeric DNA. *Nature*
885 1–5. doi:10.1038/s41586-021-03415-4

886 Grimm JB, English BP, Chen J, Slaughter JP, Zhang Z, Revyakin A, Patel R, Macklin
887 JJ, Normanno D, Singer RH, Lionnet T, Lavis LD. 2015. A general method to improve

888 fluorophores for live-cell and single-molecule microscopy. *Nat Methods* **12**:244 50–3
889 p following 250. doi:10.1038/nmeth.3256

890 Grimm JB, Xie L, Casler JC, Patel R, Tkachuk AN, Choi H, Lippincott-Schwartz J,
891 Brown TA, Glick BS, Liu Z, Lavis LD. 2020. Deuteration improves small-molecule
892 fluorophores. *Biorxiv* 2020.08.17.250027. doi:10.1101/2020.08.17.250027

893 Hansen AS, Woringer M, Grimm JB, Lavis LD, Tjian R, Darzacq X. 2018. Robust
894 model-based analysis of single-particle tracking experiments with Spot-On. *Elife* **7**.
895 doi:10.7554/elife.33125

896 Heiss NS, Girod A, Salowsky R, Wiemann S, Pepperkok R, Poustka A. 1999. Dyskerin
897 Localizes to the Nucleolus and Its Mislocalization Is Unlikely to Play a Role in the
898 Pathogenesis of Dyskeratosis Congenita. *Hum Mol Genet* **8**:2515–2524.
899 doi:10.1093/hmg/8.13.2515

900 Hyman AA, Weber CA, Jülicher F. 2014. Liquid-Liquid Phase Separation in Biology.
901 *Annu Rev Cell Dev Bi* **30**:39–58. doi:10.1146/annurev-cellbio-100913-013325

902 Jády BE, Bertrand E, Kiss T. 2004. Human telomerase RNA and box H/ACA scaRNAs
903 share a common Cajal body–specific localization signal. *J Cell Biology* **164**:647–652.
904 doi:10.1083/jcb.200310138

905 Laine RF, Tosheva KL, Gustafsson N, Gray RDM, Almada P, Albrecht D, Risa GT,
906 Hurtig F, Linds A-C, Baum B, Mercer J, Leterrier C, Pereira PM, Culley S, Henriques
907 R. 2019. NanoJ: a high-performance open-source super-resolution microscopy
908 toolbox. *J Phys D Appl Phys* **52**:163001. doi:10.1088/1361-6463/ab0261

909 Lam YW, Lamond AI. 2006. Cell Biology (Third Edition). *Part Organelles Cell Struct*
910 *Sect 1isolation Plasma Membr Organelles Cell Struct Sect 1 Isol Plasma Membr*
911 *Organelles Cell Struct* 103–107. doi:10.1016/b978-012164730-8/50087-3

912 Laprade H, Querido E, Smith MJ, Guérit D, Crimmins H, Conomos D, Pourret E,
913 Chartrand P, Sfeir A. 2020. Single-Molecule Imaging of Telomerase RNA Reveals a
914 Recruitment-Retention Model for Telomere Elongation. *Mol Cell*.
915 doi:10.1016/j.molcel.2020.05.005

916 Mitrea DM, Kriwacki RW. 2016. Phase separation in biology; functional organization of a
917 higher order. *Cell Commun Signal Ccs* **14**:1. doi:10.1186/s12964-015-0125-7

918 Nagpal N, Wang J, Zeng J, Lo E, Moon DH, Luk K, Braun RO, Burroughs LM, Keel SB,
919 Reilly C, Lindsley RC, Wolfe SA, Tai AK, Cahan P, Bauer DE, Fong YW, Agarwal S.
920 2020. Small-Molecule PAPD5 Inhibitors Restore Telomerase Activity in Patient Stem
921 Cells. *Cell Stem Cell* **26**:896-909.e8. doi:10.1016/j.stem.2020.03.016

922 Nandakumar J, Bell CF, Weidenfeld I, Zaug AJ, Leinwand LA, Cech TR. 2012. The TEL
923 patch of telomere protein TPP1 mediates telomerase recruitment and processivity.
924 *Nature* **492**:285 289. doi:10.1038/nature11648

925 Nandakumar J, Cech TR. 2013. Finding the end: recruitment of telomerase to
926 telomeres. *Nat Rev Mol Cell Bio* **14**. doi:10.1038/nrm3505

927 Riback JA, Zhu L, Ferrolino MC, Tolbert M, Mitrea DM, Sanders DW, Wei M-T, Kriwacki
928 RW, Brangwynne CP. 2020. Composition-dependent thermodynamics of intracellular
929 phase separation. *Nature* **581**:209–214. doi:10.1038/s41586-020-2256-2

930 Schmidt JC, Cech TR. 2015. Human telomerase: biogenesis, trafficking, recruitment,
931 and activation. *Gene Dev* **29**:1095 1105. doi:10.1101/gad.263863.115

932 Schmidt JC, Dalby AB, Cech TR. 2014. Identification of human TERT elements
933 necessary for telomerase recruitment to telomeres. *Elife* **3**:e03563.
934 doi:10.7554/elife.03563

935 Schmidt JC, Zaug AJ, Cech TR. 2016. Live Cell Imaging Reveals the Dynamics of
936 Telomerase Recruitment to Telomeres. *Cell* **166**:1188 1197.e9.
937 doi:10.1016/j.cell.2016.07.033

938 Schmidt JC, Zaug AJ, Kufer R, Cech TR. 2018. Dynamics of human telomerase
939 recruitment depend on template-telomere base pairing. *Mol Biol Cell* **29**:869 880.
940 doi:10.1091/mbc.e17-11-0637

941 Sergé A, Bertaux N, Rigneault H, Marguet D. 2008. Dynamic multiple-target tracing to
942 probe spatiotemporal cartography of cell membranes. *Nat Methods* **5**:687 694.
943 doi:10.1038/nmeth.1233

944 Shukla S, Jeong H-C, Sturgeon CM, Parker R, Batista LFZ. 2020. Chemical inhibition of
945 PAPD5/7 rescues telomerase function and hematopoiesis in dyskeratosis congenita.
946 *Blood Adv* **4**:2717–2722. doi:10.1182/bloodadvances.2020001848

947 Shukla S, Schmidt JC, Goldfarb KC, Cech TR, Parker R. 2016. Inhibition of telomerase
948 RNA decay rescues telomerase deficiency caused by dyskerin or PARN defects. *Nat*
949 *Struct Mol Biol* **23**:286 292. doi:10.1038/nsmb.3184

950 Southern E. 2006. Southern blotting. *Nat Protoc* **1**:518–525. doi:10.1038/nprot.2006.73

951 Stern JL, Zyner KG, Pickett HA, Cohen SB, Bryan TM. 2012. Telomerase Recruitment
952 Requires both TCAB1 and Cajal Bodies Independently. *Mol Cell Biol* **32**:2384–2395.
953 doi:10.1128/mcb.00379-12

954 Stewart SA, Weinberg RA. 2006. Telomeres: Cancer to Human Aging. *Annu Rev Cell*
955 *Dev Bi* **22**:531–557. doi:10.1146/annurev.cellbio.22.010305.104518

Stuart BD, Choi J, Zaidi S, Xing C, Holohan B, Chen R, Choi M, Dharwadkar P, Torres F, Girod CE, Weissler J, Fitzgerald J, Kershaw C, Klesney-Tait J, Mageto Y, Shay JW, Ji W, Bilguvar K, Mane S, Lifton RP, Garcia CK. 2015. Exome sequencing links mutations in PARN and RTEL1 with familial pulmonary fibrosis and telomere shortening. *Nat Genet* **47**:512 517. doi:10.1038/ng.3278

Tokunaga M, Imamoto N, Sakata-Sogawa K. 2008. Highly inclined thin illumination enables clear single-molecule imaging in cells. *Nat Methods* **5**:159 161. doi:10.1038/nmeth1171

Tomlinson RL, Ziegler TD, Supakorndej T, Terns RM, Terns MP. 2006. Cell cycle-regulated trafficking of human telomerase to telomeres. *Mol Biol Cell* **17**:955 965. doi:10.1091/mbc.e05-09-0903

Tseng C-K, Wang H-F, Burns AM, Schroeder MR, Gaspari M, Baumann P. 2015. Human Telomerase RNA Processing and Quality Control. *Cell Reports* **13**:2232–2243. doi:10.1016/j.celrep.2015.10.075

Tummala H, Walne A, Collopy L, Cardoso S, Fuente J de la, Lawson S, Powell J, Cooper N, Foster A, Mohammed S, Plagnol V, Vulliamy T, Dokal I. 2015. Poly(A)-specific ribonuclease deficiency impacts telomere biology and causes dyskeratosis congenita. *J Clin Invest* **125**:2151–2160. doi:10.1172/jci78963

Tycowski KT, Shu M-D, Kukoyi A, Steitz JA. 2009. A conserved WD40 protein binds the Cajal body localization signal of scaRNP particles. *Mol Cell* **34**:47 57. doi:10.1016/j.molcel.2009.02.020

Venteicher AS, Abreu EB, Meng Z, McCann KE, Terns RM, Veenstra TD, Terns MP, Artandi SE. 2009. A human telomerase holoenzyme protein required for Cajal body localization and telomere synthesis. *Science* **323**:644 648. doi:10.1126/science.1165357

Vogan JM, Zhang X, Youmans DT, Regalado SG, Johnson JZ, Hockemeyer D, Collins K. 2016. Minimized human telomerase maintains telomeres and resolves endogenous roles of H/ACA proteins, TCAB1, and Cajal bodies. *Elife* **5**:693. doi:10.7554/elife.18221

Wang W, Budhu A, Forgues M, Wang XW. 2005. Temporal and spatial control of nucleophosmin by the Ran–Crm1 complex in centrosome duplication. *Nat Cell Biol* **7**:823–830. doi:10.1038/ncb1282

Weidenfeld I, Gossen M, Löw R, Kentner D, Berger S, Görlich D, Bartsch D, Bujard H, Schönig K. 2009. Inducible expression of coding and inhibitory RNAs from retargetable genomic loci. *Nucleic Acids Res* **37**:e50. doi:10.1093/nar/gkp108

991 Wu RA, Upton HE, Vogan JM, Collins K. 2017. Telomerase Mechanism of Telomere
992 Synthesis. *Annu Rev Biochem* **86**:439 460. doi:10.1146/annurev-biochem-061516-
993 045019

994 Xi L, Cech TR. 2014. Inventory of telomerase components in human cells reveals
995 multiple subpopulations of hTR and hTERT. *Nucleic Acids Res* **42**:8565–8577.
996 doi:10.1093/nar/gku560

997 Zhong F, Savage SA, Shkreli M, Giri N, Jessop L, Myers T, Chen R, Alter BP, Artandi
998 SE. 2011. Disruption of telomerase trafficking by TCAB1 mutation causes
999 dyskeratosis congenita. *Gene Dev* **25**:11–16. doi:10.1101/gad.2006411

1000 Zhong FL, Batista LFZ, Freund A, Pech MF, Venteicher AS, Artandi SE. 2012. TPP1
1001 OB-Fold Domain Controls Telomere Maintenance by Recruiting Telomerase to
1002 Chromosome Ends. *Cell* **150**:481 494. doi:10.1016/j.cell.2012.07.012

1003

1004

Supplementary Information

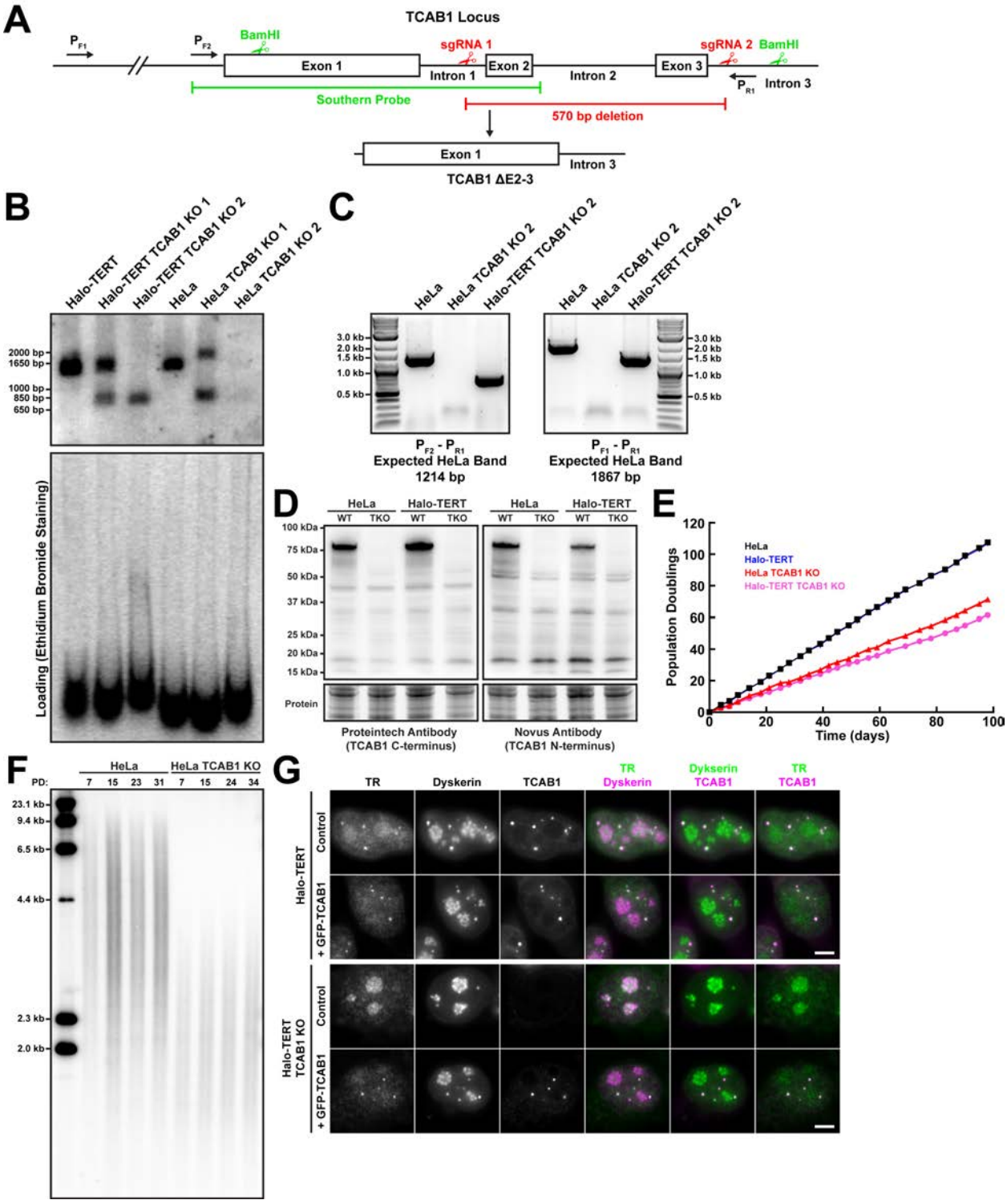

Figure 1 – Figure Supplement 1. (A) Strategy to knock-out TCAB1 using Cas9 and two sgRNAs targeting introns 1 and 3. **(B)** Southern blot of genomic DNA digested with BamHI from parental cells and TCAB1 knock-out clones using a probes generated from a PCR product of the TCAB1 gene indicated in

(A) demonstrating the expected truncation of the *TCAB1* gene in Halo-TERT TCAB1 KO 2. HeLa TCAB1 KO 2 carries larger deletions completely removing exons 1 and 2 from the *TCAB1* gene. **(C)** PCR using primers indicated in **(A)** of genomic DNA from parental cells and TCAB1 knock-out clones confirming the deletion of critical regions of the *TCAB1* gene show in **(B)**. **(D)** Western blots demonstrating the absence of TCAB1 protein in TCAB1 knock-out cell lines generated in HeLa and Halo-TERT cells lines using two antibodies targeting the N-terminus and C-terminus of TCAB1. **(E)** Growth rate of parental and TCAB1 knock-out cell lines. **(F)** Telomere length analysis by Southern blot of telomeric restriction fragments, indicating that telomeres in TCAB1 knock-out cells are short but stable in length. **(G)** Immuno-fluorescence with anti-dyskerin and anti-TCAB1 antibodies coupled to fluorescence in-situ hybridization with probes against TR, demonstrating that expression of GFP-TCAB1 in TCAB1 knock-out cells rescues TR localization to Cajal bodies (scale bar = 5 μm).

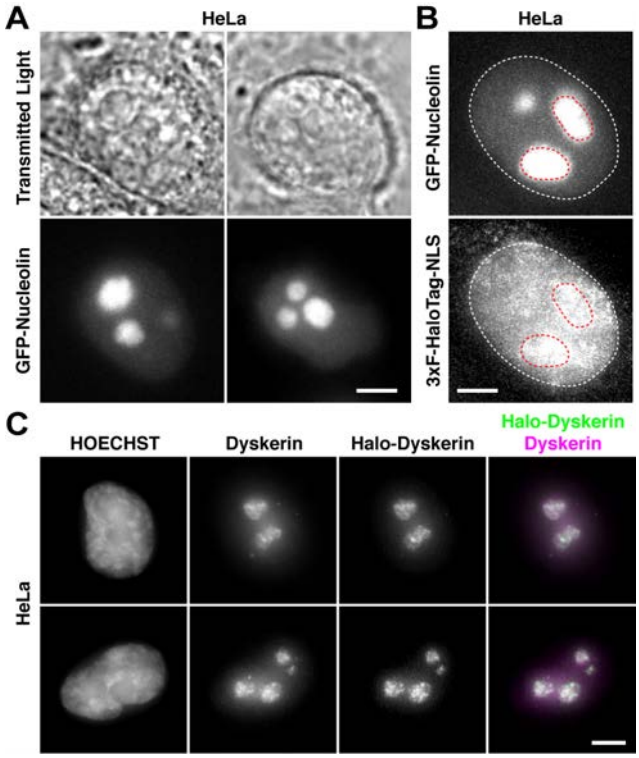

Figure 2 – Figure Supplement 1. (A) Images of HeLa cells transiently expressing GFP-nucleolin to mark nucleoli. The GFP-nucleolin signal overlaps with circular shapes visible under transmitted light illumination (scale bar = 2 μm). **(B)** Images of HeLa cells transiently expressing GFP-nucleolin and 3xFLAG-HaloTag-NLS labeled with JF646. The 3xFLAG-HaloTag-NLS signal (maximum intensity projection of 1000 frames of a single-molecule imaging movie) clearly overlaps with the GFP-nucleolin signal (red dashed outline), demonstrating that 3xFLAG-HaloTag-NLS can enter the nucleolus (scale bar = 2 μm). **(C)** Images of HeLa cells transiently expressing 3xFLAG-HaloTag-dyskerin labeled with JF646 and probed with an antibody against dyskerin, demonstrating that 3xFLAG-HaloTag-dyskerin localizes to the nucleolus (scale bar = 5 μm).

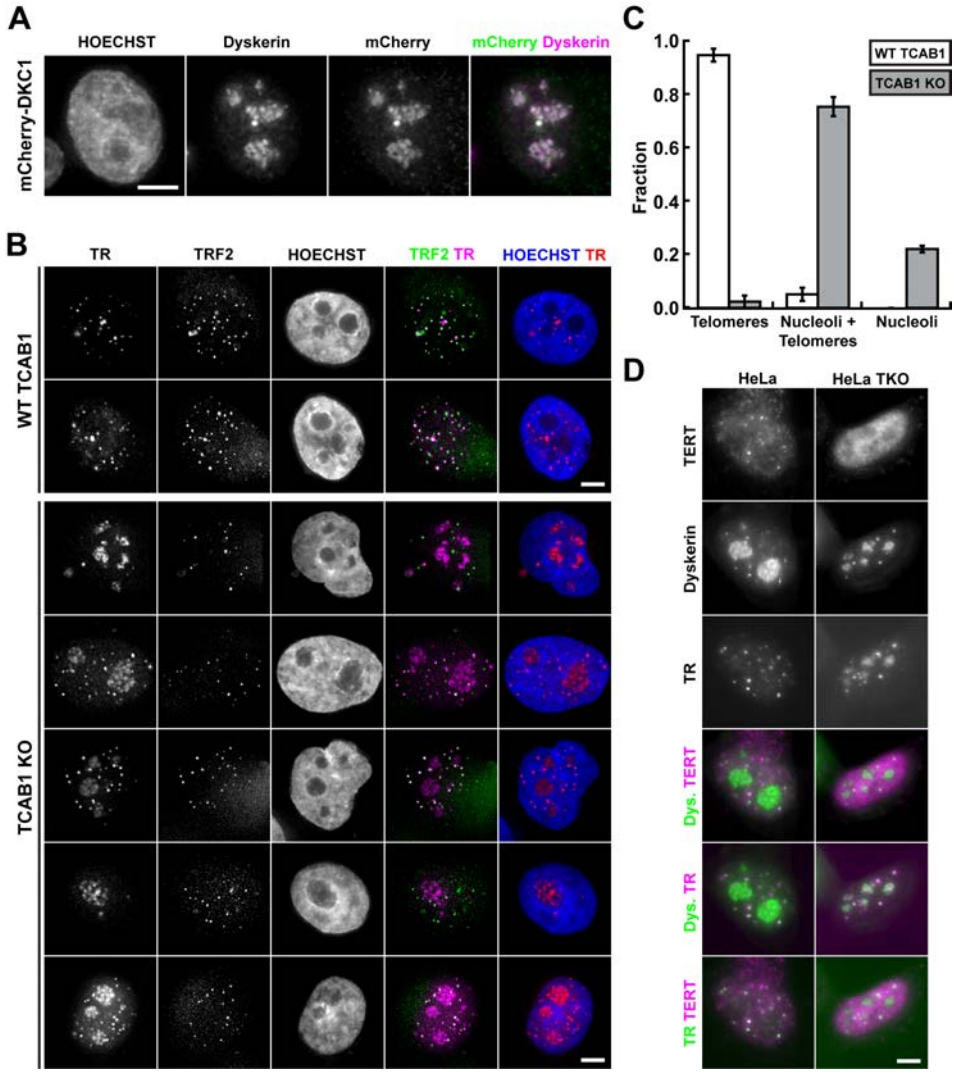

Figure 3 – Figure Supplement 1. (A) Images of HeLa cells transiently expressing mCherry-dyskerin probed with antibodies agains mCherry and dyskerin, demonstrating that mCherry dyskerin localizes to the nucleolus (scale bar = 5 μm). **(B)** Images of control and TCAB1 knock-out HeLa cells (3xFLAG-Halo-TERT, mEOS3.2-TRF2) overexpressing untagged TERT and TR. TR was detected using FISH and TRF2 was visualized using the fluorescence signal from mEOS3.2-TRF2. In control cells TR co-localizes with telomeres, while it is enriched in nucleoli and localized to telomeres in TCAB1 KO cells (scale bar = 5 μm). **(C)** Quantification of the fraction of cells showing TR localization exclusively to telomeres, to telomeres and nucleoli, or only to nucleoli (2 independent experiments, >100 cells per experiments, mean ± standard deviation). **(D)** Images of HeLa cells and TCAB1 knock-out cells transiently expressing untagged TERT and TR, probed with TERT (Abcam) and dyskerin antibodies and FISH for TR demonstrating that untagged TERT is excluded from nucleoli marked by dyskerin in parental and TCAB1 knock-out cells.

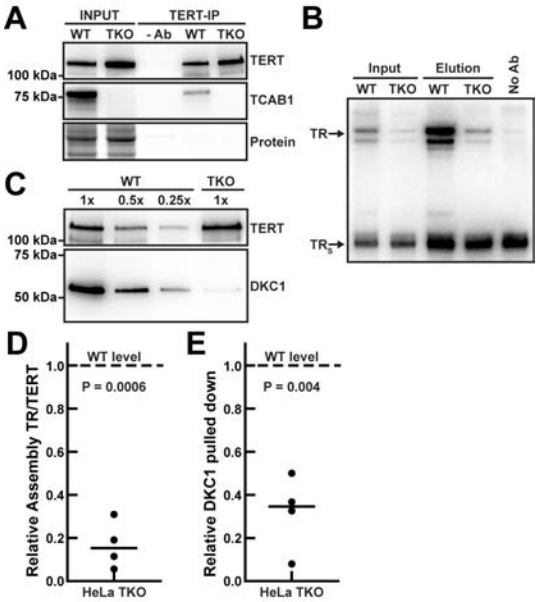

Figure 4 – Figure Supplement 1. (A) Western blots analyzing TERT immuno-purification (using a sheep anti-TERT antibody) from Halo-TERT cells overexpressing TERT and TR probed with a rabbit anti-TERT antibody (Abcam) and a TCAB1 antibody. **(B)** Northern blot of RNA extracted from input and purified TERT samples from Halo-TERT cells overexpressing TERT and TR probed with radiolabeled DNA oligonucleotides complementary to TR. Standards are *in vitro* transcribed full-length TR and truncated TR_S. TR_S was added to samples prior to RNA extraction as loading and recovery control. **(C)** Western blots to analyze immuno-purified telomerase RNP composition from Halo-TERT cells. A single membrane was cut into two pieces that were probed with TERT and dyskerin antibodies, respectively. **(D-E)** Quantification of the amount of **(D)** the ratio of TR to TERT (n = 4), and **(E)** dyskerin (n = 4) in TERT purifications from Halo-TERT TCAB1 knock-out cells overexpressing TERT and TR compared to parental controls (mean, T-Test). The dashed lines indicate the level in telomerase purified from wild-type TCAB1 control cells which was normalized to 1.0.

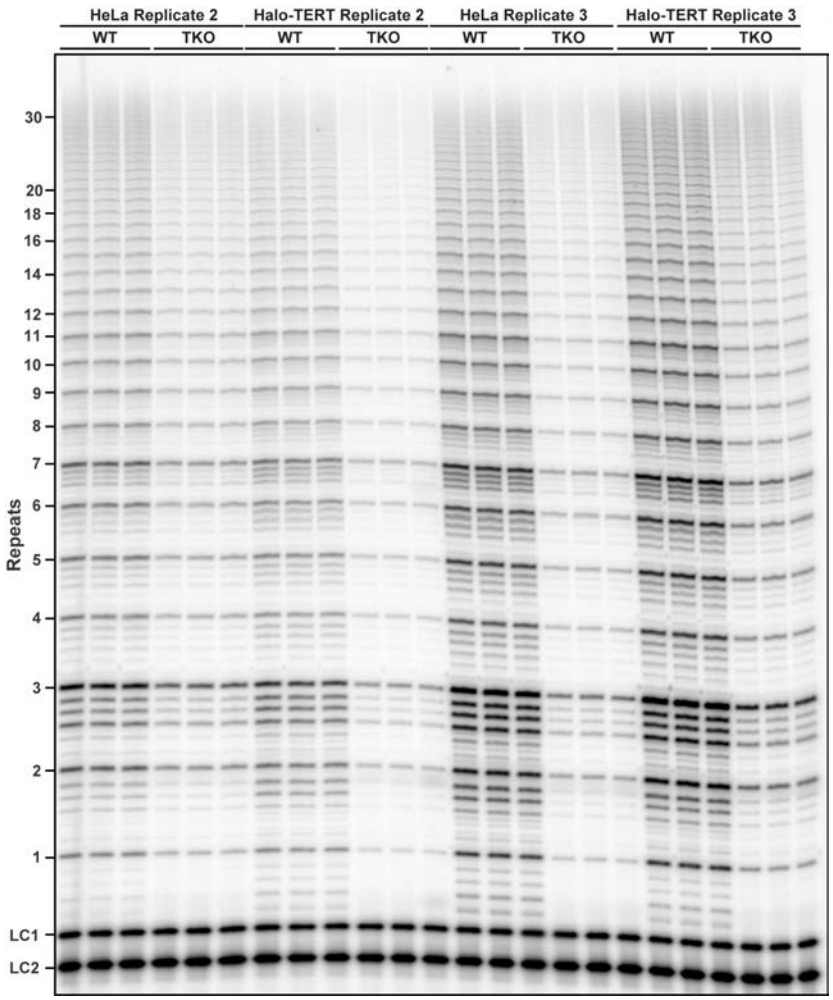

Figure 5 – Figure Supplement 1. Direct telomerase extension assay of telomerase immuno-purified from parental (WT) and TCAB1 knock-out (TKO) HeLa and Halo-TERT cell lines. LC1 and LC2, radiolabeled DNA oligonucleotide loading controls.

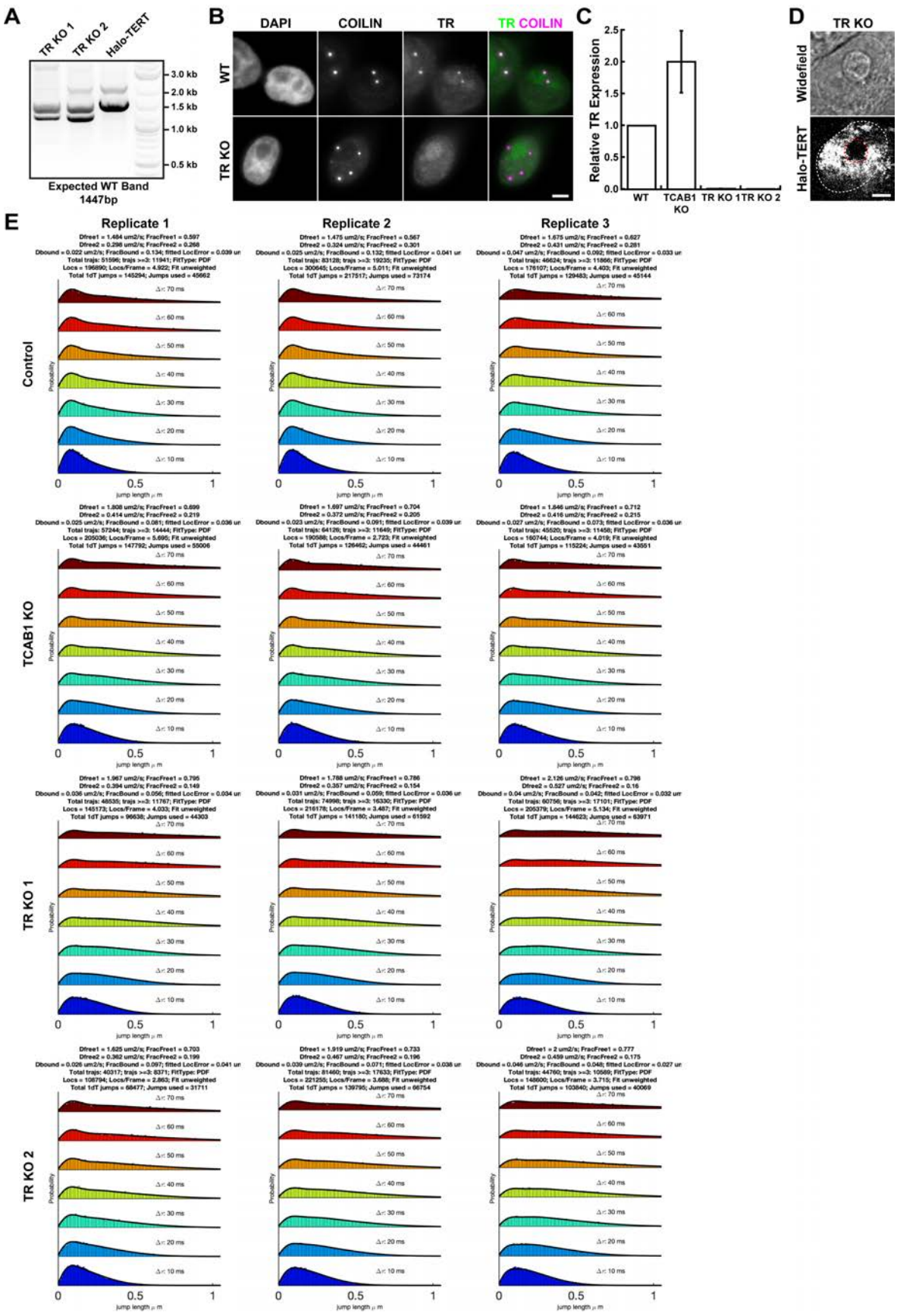

Figure 6 – Figure Supplement 1. (A) PCR analysis of the TR locus in parental and TR knock-out clones. Both TR knock-out clones show PCR products with reduced length that were confirmed to be knock-outs by Sanger sequencing. **(B)** Images of control and TR knock-out cells probed with an antibody against coilin and FISH probes specific for TR, demonstrating the lack of TR signal in TR knock-out cells (scale bar = 5 μm). **(C)** Determination of TR levels in control, TCAB1 knock-out, and TR knock-out cells, using RT-qPCR with primers specific to TR normalized to GAPDH (3 independent biological replicates, 3 technical replicates for each biological replicate, mean ± standard deviation). **(D)** Maximum intensity projection of 2000 frames of a 3xFLAG-HaloTag (JF646) TERT movie (bottom), demonstrating that the TERT signal does not overlap with the nucleolus detected as circular shape in the transmitted light image (top, red dashed line). **(E)** Fitting of single-particle tracking data of TERT from control, TCAB1 knock-out, and TR knock-out cells expressing 3xFLAG-HaloTag-TERT using the Spot-On tool.

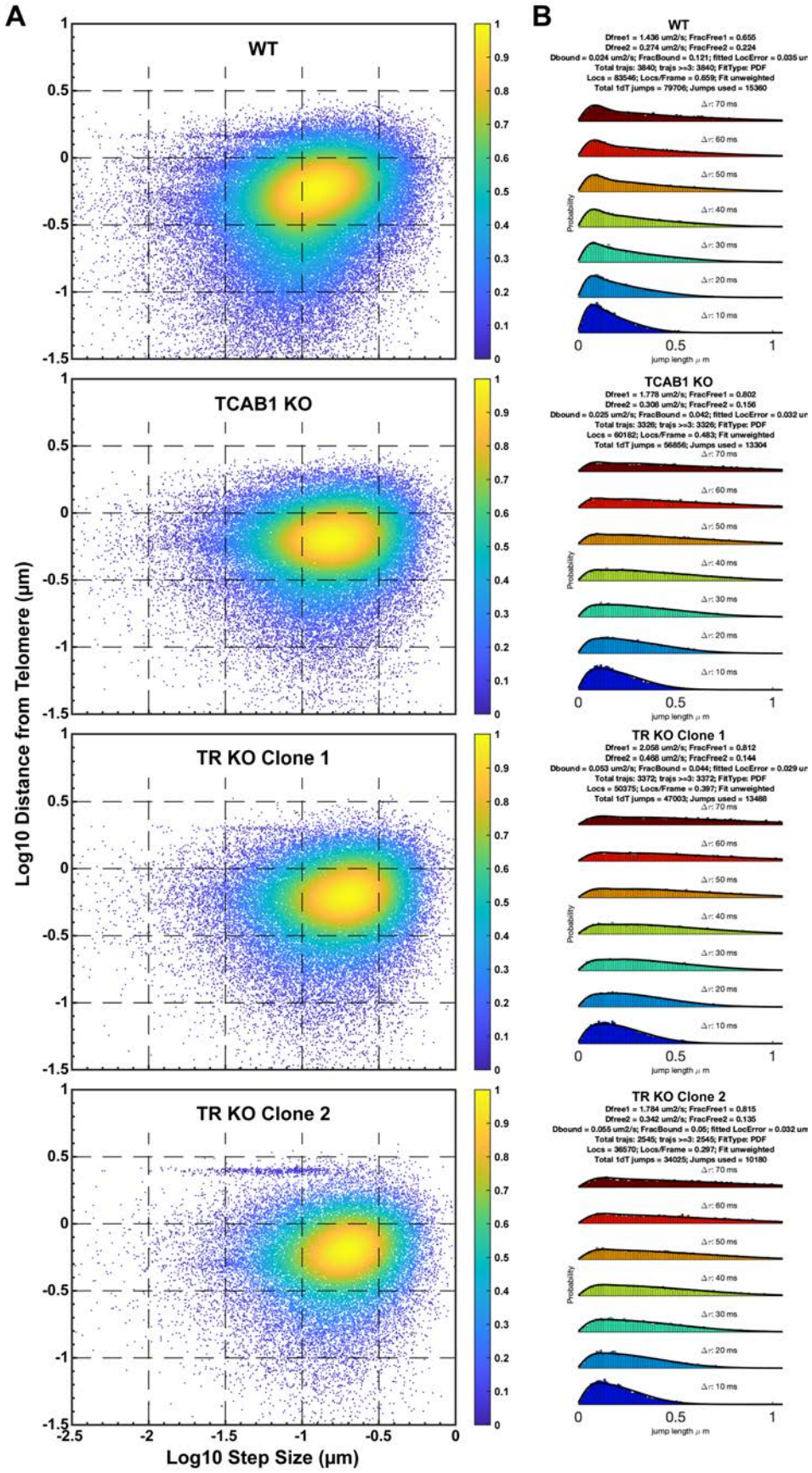

1076

Figure 6 – Figure Supplement 2. (A) Analysis if the step size of telomeric TERT particles relative to the distance of the particle to the closest telomere (pooled results from 3 independent biological replicates with 19-30 cells analyzed per replicate). TERT molecules bound to the telomere are expected to have small step sizes and a short distance to the closest telomere, which is apparent in the enrichment of events in the lower quadrants in the WT control. This enrichment is not observed in TCAB1 and TR knock-out cells. **(B)** Spot-On analysis of telomeric TERT particles (pooled results from 3 independent biological replicates with 19-30 cells analyzed per replicate). The fraction of bound TERT particles in TCAB1 and TR knock-out cells is 4-5%, compared to 12% in the WT control cells.

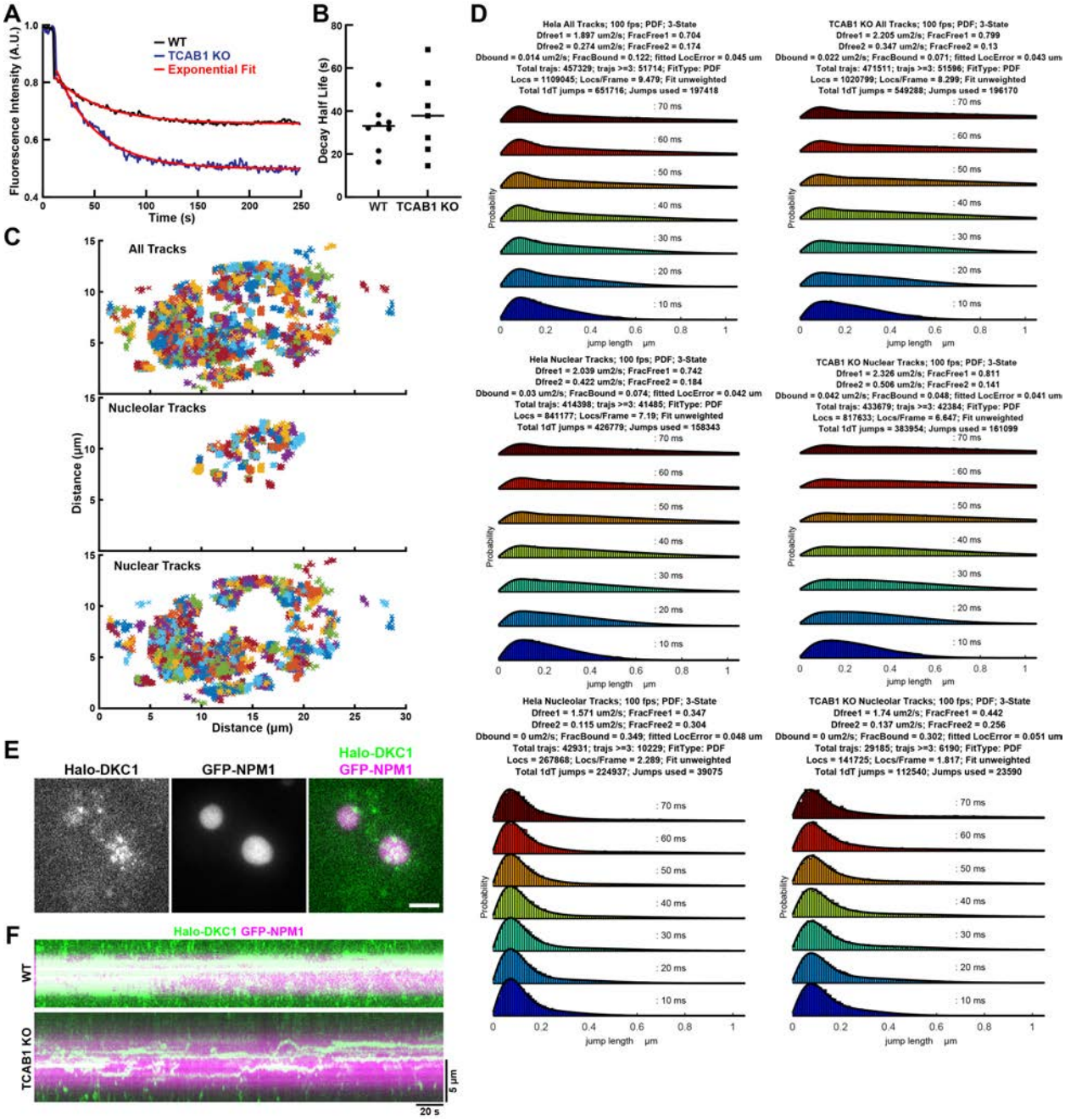

Figure 7 – Figure Supplement 1. (A) Fluorescence recovery curves of nucleolar dyskerin in the inbleached nucleolus of control and TCAB1 knock-out cells. Data was fit with a single exponential function. **(B)** Quantification of half-life of fluorescence recovery, calculated from the rate constant of the single exponential fit of the data shown in **(A)** (n = 8 and 7, mean). **(C)** Trajectories of all (top), nucleolar (middle),

and nucleoplasmic dyskerin particles. **(D)** Spot-On analysis of dyskerin diffusion of all (top), nucleolar (middle), and nucleoplasmic dyskerin particles. **(E)** Fluorescence images of single 3xFLAG-HaloTag-dyskerin particles, and nucleoli marked by GFP-NPM1 in a cell imaged at 1 frame per second (scale bar = 5 μm). **(F)** Kymographs of nucleolar 3xFLAG-HaloTag-dyskerin particles imaged at 1 frame per second.

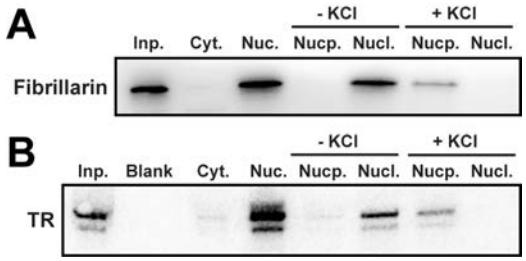

Figure 8 – Figure Supplement 1. (A) Western blot and **(B)** Northern blot of cellular fractions from TCAB1 knock-out cells probed with an antibody against fibrillarin and probes for TR, respectively. Ruptured nuclei were either maintained at a low salt concentration or exposed to 357.5 mM KCl. The results demonstrate that nucleoli are dissolved in the presence of a high salt concentration, releasing fibrillarin and TR into the nucleoplasmic fraction.

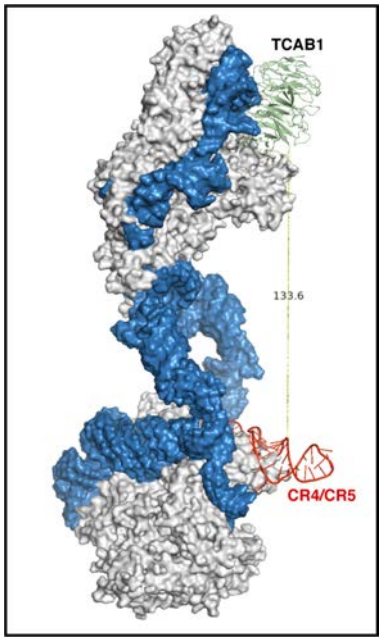

Figure 8 – Figure Supplement 2. (A) Structure of the telomerase RNP showing the distance between TCAB1 and CR4/CR5 (13.4 nm). TR in blue, CR4/CR5 in red, and TCAB1 in green (Ghanim et al., 2021).

Movie Legends

Movie 1. Single-particle tracking of 3xFLAG-HaloTag-TERT labeled with JF646 in a control cell acquired at 100 frames per second. Trajectories with a minimum of 5 localizations are displayed. 150x150 pixels with a pixel size of 0.16 μm.

Movie 2. Single-particle tracking of 3xFLAG-HaloTag-TERT labeled with JF646 in a TCAB1 knock-out cell acquired at 100 frames per second. Trajectories with a minimum of 5 localizations are displayed. 150x150 pixels with a pixel size of 0.16 μm.

Movie 3. Movie of cell expressing GFP-nucleolin (red) and 3xFLAG-HaloTag-NLS (green) labeled with JF646 acquired at 100 frames per second, showing overlap of 3xFLAG-HaloTag-NLS with nucleoli. 140x140 pixels with a pixel size of 0.16 μm.

Movie 4. Movie of 3xFLAG-HaloTag-TERT labeled with JF646 in a control (left), TCAB1 knock-out (middle), and TR knock-out (right) cell acquired at 100 frames per second. Each panel is 150x150 pixels in size with a pixel size of 0.16 μm.

Movie 5. Single-particle tracking of 3xFLAG-HaloTag-TERT labeled with JF646 in a TR knock-out cells acquired at 100 frames per second. Trajectories with a minimum of 5 localizations are displayed. 150x150 pixels with a pixel size of 0.16 μm.

Movie 6. Fluorescence recovery after photobleaching of HaloTag-dyskerin labeled with JFX650 HaloTag-ligand expressed in control cells acquired at 1 frame per second.

Movie 7. Fluorescence recovery after photobleaching of HaloTag-dyskerin labeled with JFX650 HaloTag-ligand expressed in TCAB1 knock-out cells cells acquired at 1 frame per second.

Movie 8. Movie of cells expressing GFP-nucleolin (magenta) and HaloTag-dyskerin labeled with JFX650 (green) in control cells acquired at 100 frames per second.

Movie 9. Movie of cells expressing GFP-nucleolin (magenta) and HaloTag-dyskerin labeled with JFX650 (green) in control cells acquired at 1 frame per second.